TÜBİTAK

**Turkish Journal of Earth Sciences**

**http://journals.tubitak.gov.tr/earth/**

**Research Article**

Turkish J Earth Sci
(2016) 25: 19-45

doi:10.3906/yer-1501-36

# Late Quaternary paleoceanographic evolution of the Aegean Sea: planktonic foraminifera and stable isotopes

**Ekrem Bursin İŞLER, Ali Engin AKSU*, Richard Nicholas HISCOTT**
Department of Earth Sciences, Centre for Earth Resources Research, Memorial University of Newfoundland, St. John's, Newfoundland, Canada

**Received:** 29.01.2015 • **Accepted/Published Online:** 19.11.2015 • **Final Version:** 01.01.2016

**Abstract:** Aspects of the paleoclimatic and paleoceanographic evolution of the Aegean Sea since ~130 ka are revealed by quantitative variations in planktonic faunal assemblages, the $\delta^{18}O$ and $\delta^{13}C$ isotopic composition of benthic and planktonic foraminifera, and Mg/Ca ratios in planktonic foraminifera extracted from five 6–10-m-long piston cores. Independent sea surface temperature (SST) estimates obtained using planktonic foraminiferal transfer functions and the Mg/Ca ratios show excellent agreement, with $r^2$ correlation coefficients of 0.92–0.95. Planktonic foraminiferal assemblages are similar, through time, across several deep basins, suggesting that major changes must have occurred in near synchroneity across the Aegean Sea. The data suggest that sapropels S3, S4, and S5 were deposited under a stratified water column during times of increased primary productivity and the development of a deep chlorophyll maximum layer. Under such conditions, oxygen advection via intermediate water flow must have been significantly reduced, in turn implying bottom water stagnation. Sapropel S1 lacks a deep phytoplankton assemblage; this faunal contrast between S1 and older sapropels indicates that S1 must have been deposited in the absence of a deep chlorophyll maximum layer.
Cluster analysis shows a consistent coupling of *Globigerina bulloides* with *Globigerinoides ruber* during times of nonsapropel deposition, interpreted to require a stratified euphotic zone composed of a warm, nutrient-poor upper layer and a cooler, nutrient-rich lower layer. The covariation of these two species suggests increased river runoff that controlled the fertility and stratification of the surface waters.

**Key words:** Sapropel, planktonic foraminifera, SST, oxygen and carbon isotopes, Mg/Ca ratios, Quaternary, paleoclimate, paleoceanography, Aegean Sea

## 1. Introduction

Planktonic foraminifera are powerful indicators of water-mass characteristics in Pleistocene–Recent paleoceanographic studies (e.g., Rohling et al., 2004). Qualitative and quantitative studies show that planktonic foraminifera have both geographic and water-depth preferences, occupying distinct ecological niches controlled by the water-mass properties, and upwelling (e.g., Sautter and Thunell, 1991). Variations in oxygen and carbon isotopic compositions and trace-element ratios (e.g., Mg/Ca) in foraminiferal tests are reliable indicators of sea-surface and bottom-water temperatures and salinities, as well as the availability of food in the water column (e.g., Lea et al., 2003; Rohling et al., 2004; Geraga et al., 2005). Temporal changes can be tracked using downcore variations of planktonic foraminiferal assemblages, with distinctive assemblages assigned to separate 'ecozones' (e.g., Capotondi et al., 1999).

Many species of planktonic foraminifera host a variety of photoautotrophs, including dinoflagellates, diatoms, green algae, red algae, chrysophytes, and prymnesiophytes; these symbiont-bearing planktonic foraminifera are better adapted to a wider range of light conditions (e.g., colour spectrum) and water depths in the oceans (Bé et al., 1982, Hemleben et al., 1989, Edgar et al., 2013). The symbiont plays a critical role in nutrition, reproduction, calcification, growth, and longevity of the host organism (Edgar et al., 2013). Symbiont-bearing planktonic foraminifera are widespread and abundant across the euphotic zone in subtropical and tropical oceans where food concentrations and water temperatures and salinities can show large vertical variations. Distinct planktonic foraminiferal assemblages occur in such environments, largely controlled by the specific temperature, salinity, nutrient, and dissolved oxygen preferences of the constituent species (Hemleben et al., 1989). Symbiont-bearing planktonic foraminiferal species often show diurnal and ontogenetic vertical migration patterns in the water column, and sink into deeper waters during reproduction (Hemleben et

* Correspondence: aaksu@mun.ca

al., 1989). In contrast, nonsymbiont-bearing planktonic foraminiferal species, such as *Neogloboquadrina dutertrei*, *G. bulloides*, and *Globorotalia inflata*, are not restricted to the euphotic zone and are often found at greater depths in the oceans (Bé et al., 1982, Hemleben et al., 1989).

There has been particular interest in the planktonic foraminifera species *G. ruber* (white), which indicates warm/oligotrophic summer mixedlayer conditions (e.g., Rohling et al., 1993; Reiss et al., 1999); *Neogloboquadrina pachyderma* (dextral) and *N. dutertrei*, which are intermediate water dwellers and may suggest shoaling of the pycnocline into the base of the euphotic layer to create a distinct deep chlorophyll maximum; *G. bulloides*, which indicates eutrophic surface waters such as seen in upwelling zones, and *G. inflata* and/or *Globorotalia scitula*, which reflect a cool, homogeneous, and relatively eutrophic winter mixed layer (Reis et al., 1999; Rohling et al., 2004).

This paper uses planktonic foraminiferal assemblages, $\delta^{18}O$ records in planktonic and benthic foraminifera, and Mg/Ca ratios in planktonic foraminiferal tests extracted from five piston cores from the Aegean Sea. Objectives are (i) to delineate the Late Quaternary paleoceanographic evolution of the region, with special emphasis on the determination of sea-surface temperature and salinity variations during the accumulation of organic-rich sediments (i.e. sapropels and sapropelic muds, Kidd et al., 1978) and nonsapropelic background sediments and (ii) to examine temporal and spatial variations in the characteristics of the water column, in particular the degree of stratification and temporal variations in the depth and strength of the pycnocline. Little has been published about sediments older than 20–28 ka in the Aegean Sea (e.g., Casford et al., 2002; Geraga et al., 2008, 2010). Therefore, the paleoclimatic and paleoceanographic history of this important gateway between the Black Sea and the eastern Mediterranean Sea is, to a large extent, limited to conditions following the last glacial maximum (LGM). The core data presented in this paper provide a much needed record of Aegean Sea paleoclimate and paleoceanography prior to the LGM, in particular before Marine Isotopic Stage (MIS) 2.

### 1.1. Seabed morphology and hydrography of the Aegean Sea

The Aegean Sea is a shallow elongate embayment that forms the northeastern extension of the eastern Mediterranean Sea (Figure 1). To the northeast, it is connected to the Black Sea through the straits of Dardanelles and Bosphorus and the intervening small land-locked Marmara Sea. In the south, the Aegean Sea communicates with the eastern Mediterranean Sea through several broad and deep straits located between the Peloponnesus Peninsula, the Island of Crete, and southwestern Turkey (Figure 1). The Aegean Sea is divided into three physiographic regions (*italics*): the northern Aegean Sea, including the North Aegean Trough; the central Aegean plateaux and basins; and the southern Aegean Sea, including the Cretan Trough.

The dominant bathymetric feature in the northern portion of the Aegean Sea is the 800–1200-m-deep depression known as the North Aegean Trough. It includes several interconnected depressions and extends WSW–SW from Saros Bay, widening toward the west (Figure 1). The central Aegean Sea is characterized by a series of shallower (600–1000 m), mainly NE-oriented depressions and their intervening 100–300-m-deep shoals and associated islands (Figure 1; Yaltırak et al., 2012). Five cores were collected from the central Aegean Sea, specifically from the North Skiros, Euboea, Mikonos, and North and South Ikaria basins (Figure 1). Regional studies have shown that normal faulting and strike-slip faulting are the two dominant mechanisms controlling seabed morphology in the Aegean Sea, both tied to the complex interactions of the west-propagating strands of the North Anatolian Fault and crustal extension across the Aegean region caused by slab roll-back beneath the Hellenic Arc (e.g., Yaltırak et al., 2012). The North Skiros and Euboea basins are small, 500-1000-m-deep, fault-bounded depressions south of the North Aegean Trough (Figure 1; Yaltırak et al., 2012). The North and South Ikaria basins are also small fault-bounded depressions, 650–1000 m deep, situated north and south of the Island of Ikaria, respectively.

The southern Aegean Sea is separated from the central Aegean Sea by the arcuate Cyclades, a convex-southward volcanic arc that is mostly shallowly submerged as shoals surrounding numerous islands extending from the southern tip of Euboea Island to southwestern Turkey (Figure 1). A large, 1000–2000-m-deep, generally E–W-trending depression, the Cretan Trough, occupies the southernmost portion of the Aegean Sea immediately north of Crete (Figure 1).

The continental shelves surrounding the Aegean Sea are generally narrow (1–10 km) in the west, but wider (25–95 km) in the east and north where medium-size rivers enter the sea (Figure 1). The shelf-to-slope break occurs between 100 m and 150 m water depth, largely coincident with basin-bounding faults. Steep slopes (to 1:20) lead into the small and relatively deep North Skiros, Euboea, Mikonos, North Ikaria, and South Ikaria basins. There is no clear shelf-to-slope break around the scattered islands of the Aegean Sea, where the sea floor displays linear shore-parallel troughs and ridges (Yaltırak et al., 2012). The broadest shelves occur in front of deltas off the mouths of present-day rivers in the eastern and northern Aegean Sea, and at the outlet of the Strait of Dardanelles in the northeastern Aegean Sea.

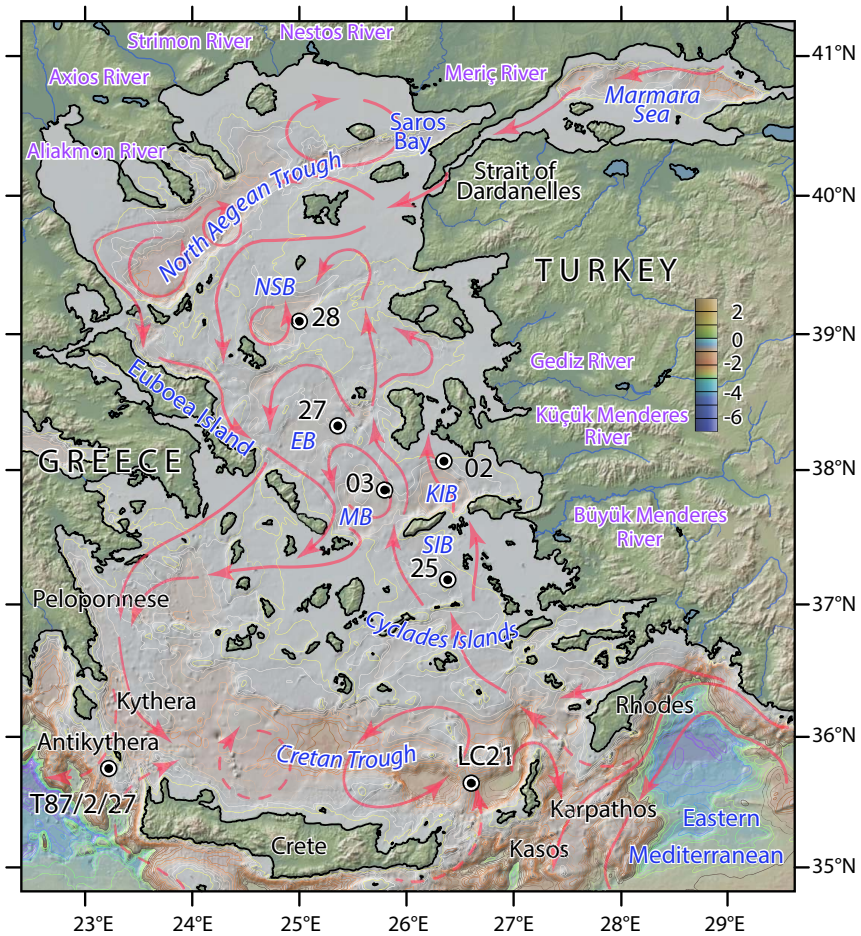


**Figure 1.** Morphological map of the Aegean Sea and surroundings, the locations of cores used in this study, and the locations of cores LC21 and T87/2/27 (discussed in text), and major rivers. Bathymetric contours are at 200 m intervals, and darker tones in the Aegean Sea indicate greater water depths. NSB = North Skiros Basin, EB = Euboea Basin, MB = Mikonos Basin, NIB = North Ikaria Basin, SIB = South Ikaria Basin. Core names are abbreviated: 02 = MAR03-02, 03 = MAR03-03, 25 = MAR03-25, 27 = MAR03-27, 28 = MAR03-28. Red arrows = surface water circulation from Olson et al. (2006) and Skliris et al. (2010). Elevation scale in kilometers.

The physical oceanography of the Aegean Sea is controlled by the regional climate, the freshwater discharge from major rivers draining southeastern Europe, and seasonal variations in the Black Sea surface-water outflow through the Strait of Dardanelles. Previous studies reveal a general cyclonic water circulation in the Aegean Sea, on which is superimposed a number of mesoscale cyclonic and anticyclonic eddies (Casford et al., 2002). A branch of the westward-flowing Asia Minor Current deviates toward the north from the eastern Mediterranean basin, carrying the warm (16–25 °C) and saline (39.2–39.5 psu) Levantine Surface Water and Levantine Intermediate Water along the western coast of Turkey. These water masses occupy the uppermost 400 m of the water column. The Asia Minor Current reaches the northern Aegean Sea where it encounters the relatively cool (9–22 °C) and less saline (22–23 psu) Black Sea Water and forms a strong thermohaline front. As a result, the water column structure in the northern and central Aegean Sea comprises a 20–70-m-thick surface veneer consisting of modified Black Sea Water overlying higher salinity Levantine Intermediate Water that extends down to 400 m. The water column below 400 m is occupied by the locally formed North Aegean Deep Water with uniform temperature (13–14 °C) and salinity (39.1–39.2 psu; Zervakis et al., 2000, 2004; Velaoras and Lascaratos, 2005). The surface and intermediate waters follow the general counter-clockwise circulation of the Aegean Sea, and progressively mix as they flow southwards along the east coast of Greece.

There are several moderate-size rivers that discharge into the Aegean Sea, including the Meriç, Nestos, Strimon, Axios, and Aliakmon rivers in the north, and the Gediz and Büyük and Küçük Menderes rivers in the east (Figure 1). These rivers drain southeastern Europe and western Turkey with a combined average annual discharge of ~1400 $m^3$ $s^{-1}$, and an average annual sediment yield of ~229 × $10^6$ t (Aksu et al., 1995). Most of this sediment is trapped on the shelves, but considerable quantities bypass the shelf edge, accounting for high sedimentation rates of 10–30 cm $kyr^{-1}$ in deeper basins (e.g., İşler et al., 2008). The Aegean Sea also receives large quantities of Black Sea surface water at an average rate of ~400 $km^3$ $yr^{-1}$ through the Strait of Dardanelles. Most of this outflow occurs during the late spring and summer, closely correlating with the maximum discharge of large European rivers draining into the Black Sea. However, nearly all the sediments carried by these rivers are stored in the Black Sea.

## 2. Materials and methods

Several long piston and gravity cores were collected from the Aegean Sea during the MAR03 cruise of the *RV Koca Piri Reis* using a 12-m-long Benthos piston corer (1000 kg head weight) triggered by a 3-m-long gravity corer (Figure 1; Table 1). The amount of core penetration was estimated by the mud smear along the core barrels, and subsequently compared with the actual core recovery. The gravity cores were used to determine and quantify potential core-top loss during the piston coring operation. All cores were kept upright onboard and during transport to Canada. Cores were split and described at Memorial University of Newfoundland. Sediment colour was determined using the "Rock-Color Chart" published by the Geological Society of America in 1984. Five key cores were sampled at 10-cm intervals. Approximately 7-$cm^3$ and 13-$cm^3$ sediment samples were collected for stable-isotopic and faunal studies, respectively.

Planktonic foraminifera were studied in five cores. Samples were dried in a 40 °C oven for 48 h, weighed, transferred to glass beakers, and disaggregated in 100 $cm^3$ of distilled water containing 15 $cm^3$ of 1% Calgon (Na-hexametaphosphate) and 10 $cm^3$ of 30% hydrogen peroxide. Next, samples were wet sieved through a 63 μm sieve, dried in a 40 °C oven, and the >63 μm fractions were stored in glass vials. Each sample was subsequently dry-sieved through 150 and 500 μm sieves. The 150–500 μm fractions were divided into aliquots using a microsplitter until each subsample contained no less than 300 planktonic foraminiferal tests. Each aliquot was then transferred to a cardboard counting slide. All planktonic foraminifera were identified and counted in each subsample. The taxa identified in the subsamples were converted into percentages of the total number of planktonic foraminifera. Identifications follow the taxonomic descriptions reported by Parker (1962), Saito et al. (1981), and Hemleben et al. (1989). The total planktonic foraminiferal abundances in each sample were calculated as 'number of specimens per dry-weight sediment'.

Sea-surface temperature (SST) and sea-surface salinity (SSS) were calculated from each sample's planktonic foraminiferal assemblage using the transfer function technique developed by Imbrie and Kipp (1971), and the functional relationships of Thunell (1979). The standard errors for the summer and winter SST are 1 °C and 1.2 °C, respectively. The SST and SSS values obtained using the planktonic foraminiferal transfer function compare well with CTD casts acquired during two field seasons (Table 2), although the summer SST values from the transfer function results are slight overestimates. However, these SST estimates are within the annual range of water temperatures in the Aegean Sea.

For oxygen isotopic analyses, the planktonic foraminifera *Globigerinoides ruber* and the benthic foraminifera *Uvigerina mediterranea* were used. For a few samples, where *G. ruber* was absent, *Globigerina bulloides* was picked instead. For planktonic foraminifera, the oxygen and carbon isotopic values of both *G. ruber* and *G. bulloides* are plotted using different colours and scales (see Appendices 1 and 2). There are 30 samples in which both *G. ruber* and *G. bulloides* were analysed: these samples show a clear and remarkably consistent offset. The oxygen and carbon isotopic data were replotted (the middle column;

**Table 1.** Location and water depth of cores used in this study. A = length of piston core, B = length of gravity core, C = amount of core top loss during coring, D = length of the composite core. Navigation is obtained using a global positioning system.

| Core | Latitude | Longitude | A (cm) | B (cm) | C (cm) | D (cm) | Water (m) |
|---|---|---|---|---|---|---|---|
| MAR03-02 | 38°03.97′N | 26°22.30′E | 776 | 86 | 37 | 813 | 398 |
| MAR03-03 | 37°51.72′N | 25°49.17′E | 580 | 50 | 24 | 604 | 720 |
| MAR03-25 | 37°10.36′N | 26°26.55′E | 604 | 25 | 25 | 629 | 494 |
| MAR03-27 | 38°18.68′N | 25°18.97′E | 952 | 106 | 80 | 1032 | 651 |
| MAR03-28 | 39°01.02′N | 25°01.48′E | 726 | 165 | 100 | 826 | 453 |

**Table 2.** Comparison between the sea surface temperatures and salinities obtained using the planktonic foraminiferal transfer function and the summer sea surface temperatures and salinities obtained in CTD casts during cruises in 1991 (Aksu et al., 1995b) and 2003 (Institute of Marine Sciences and Technology, Dokuz Eylül University, unpublished data).

| | 2003 (°C) | 2003 (psu) | 1991 (°C) | 1991 (psu) | SSTw (°C) | SSTw (°C) |
|---|---|---|---|---|---|---|
| MAR03-02 | 23.44 | 39.79 | 24.55 | 39.43 | 18.99 | 27.17 |
| MAR03-03 | 23.92 | 39.50 | 24.55 | 39.42 | 18.99 | 27.17 |
| MAR03-25 | 21.55 | 39.70 | 23.56 | 39.35 | 18.08 | 25.75 |
| MAR03-27 | 22.50 | 39.57 | 23.44 | 39.23 | 18.99 | 27.33 |
| MAR03-28 | 23.43 | 39.28 | 24.53 | 39.15 | 19.38 | 27.61 |

Appendices 1 and 2) by shifting the *G. bulloides* curve by ~1 permil, but clearly showing a scale for *G. bulloides* for clarity. Then a pseudocomposite section was created, but showing the isotopic values for both *G. ruber* and *G. bulloides* with separate horizontal scales and different colours. This pseudocomposite plot is carried forward into figures in the main text that require the oxygen and carbon isotopic records of cores M03-27 and M03-28. The reader is reminded that (with separate isotope scales and colours) two species were used in these two cores. In each sample 15–20 *G. ruber* and 4–6 *U. mediterranea* (or 15–20 *G. bulloides*) were hand-picked from the >150 μm fractions, cleaned in distilled water, and dried in an oven at 50 °C. The foraminiferal samples were then placed in 12 mL autoinjector reaction vessels. The reaction vessels were covered with Exetainer screw caps with pierceable septa, and were placed in a heated sample holder held at 70 °C. Using a GC Pal autoinjector, the vials were flushed with ultrahigh purity He for 5 min using a double-holed needle connected by tubing to the He gas source. Sample vials were then manually injected with 0.1 mL of 100% $H_3PO_4$ using a syringe and needle. A minimum of 1 h was allowed for carbonate samples to react with the phosphoric acid. The samples were analysed using a triple collector Thermo Electron Delta V Plus isotope ratio mass spectrometer. Reference gases were prepared from three different standards of known isotopic composition using the same methods employed for the unknown samples, and were used to calibrate each run. The $\delta^{18}O$ and $\delta^{13}C$ values are reported with respect to the Pee Dee Belemnite (PDB) standard.

For trace-element measurements on foraminifera, 10–15 tests were placed in a small vial with distilled water and cleaned using an ultrasonic cleaner for 30 s, then rinsed, and dried in an oven at 40 °C. Five specimens of *G. ruber* from each sample were mounted on 2.5 × 5 cm glass slides with double-sided sticky tape, with the aperture facing upwards. Mg and Ca concentrations in the carbonate foraminiferal tests were obtained using a Finnigan ELEMENT XR, a high-resolution double-focussing magnetic-sector inductively coupled plasma mass spectrometer (HRICPMS), and a GEOLAS excimer laser (λ = 193 nm) at Memorial University of Newfoundland. The laser was focussed on the sample and fired at 5 Hz repetition rate using an energy density of 5 J/cm$^2$ and 59 μ laser spot diameter. Between 5 and 6 pits were laser-ablated for each *G. ruber* specimen, with no more than 2 pits on a single chamber. Thus, an average of 30 ablations (5 specimens × 6 ablations) was carried out in each sample. The results are expressed as Mg/Ca (mmol/mol) ratio. Standard deviation of the Mg content in *G. ruber* tests is calculated to be approximately 0.02 μg based on replicate measurements on a number of randomly selected samples at several depths from cores MAR03-28 and MAR03-02. Mg/Ca temperature calculations were performed using the equation $Mg/Ca = 0.34^{0.102 \times T}$ from Anand et al. (2003). This equation is preferred because it was constructed for *G. ruber* (white) (250–350 μm), which is the same species and size range used in this study. Due to the logarithmic nature of the Mg/Ca temperature equation, cooler temperatures (low Mg content) are associated with larger error bars. The standard errors for cores MAR03-28 and MAR03-02 are, respectively, 1.7–6.8 °C and 1.4–5 °C, with an average of 3 °C and 2.5 °C.

Stacked planktonic and benthic oxygen and carbon isotope curves were constructed by averaging the isotopic values in cores MAR03-02, MAR03-03, MAR03-25, MAR03-27, and MAR03-28. The 0–110 ka portions of the stacked planktonic curves were constructed using the average isotopic values of only *G. ruber* in cores MAR03-02, MAR03-28, and MAR03-27. The sections corresponding to 110–130 ka are the $\delta^{18}O$ and $\delta^{13}C$ curves from core MAR03-28. The 0-110 ka portions of the stacked benthic isotope curves were constructed using the average isotopic values in cores MAR03-02, MAR03-03, MAR03-25, and MAR03-28. The sections pertaining to 110–130 ka are the average of the isotopic values in cores MAR03-03 and MAR03-28.

## 3. Results

### 3.1. Lithostratigraphy

On the basis of visual core descriptions, organic carbon content, and colour, four sapropel and five nonsapropel units are identified and labeled as 'A' through 'I' from top to bottom (Figure 2). The correlation of the units among the five cores (Figure 3) was accomplished by matching peaks of oxygen isotopic curves together with the stratigraphic positions of geochemically fingerprinted ash layers (Aksu et al., 2008). Throughout the cores, sapropel units are distinguished by their darker colors and higher organic carbon contents. However, rather than a fixed quantitative threshold (e.g., >0.5%, >1%, or >2% TOC content), an organic carbon content twice (or more) that of the underlying and overlying units was used to classify a lithostratigraphic unit as a sapropel. Using this criterion, sediments with 1.0%–12.65% TOC content are described in this paper as sapropels. Most sediments consist of clay/silt mixtures that are slightly to moderately burrowed. The coarse fraction is mainly foraminifera, pteropods, bivalve, and gastropod shells, and variable amounts of volcanic ash. Sediment accumulation is inferred to have occurred through hemipelagic rain due to paucity of terrigenous sand-sized material, lack of evidence for resedimentation as normally graded beds, and ubiquitous bioturbation.

Nonsapropel units A, C, E, G, and I are composed of burrow-mottled foraminifera-bearing calcareous clayey mud. The units are predominantly yellowish to dark yellowish brown (10YR5/4, 10YR4/2) and various shades of gray (i.e. yellowish, light, and dark; 5Y5/2, 5Y6/1, 5GY6/1). The TOC content is 0.4%–0.7% (average 0.5%) with higher organic carbon contents in unit G reaching 0.9% (Figure 2). Unit A contains an ash layer largely disseminated in fine mud. The ash is widespread throughout the Aegean Sea and has been identified by geochemical fingerprinting as the Z2 tephra from the Minoan eruption of Santorini Island (Aksu et al., 2008).

Unit C contains three tephra layers which are described in detail by Aksu et al. (2008), and identified by those authors using geochemical fingerprinting. From top to bottom they are the Y2 tephra (the Cape Riva eruption on the Island of Santorini also known as the Akrotiri eruption), the Y5 tephra (Campanian Ignimbrite eruption of the Phlegran Fields of the Italian Volcanic Province), and the Nisyros tephra (Nisyros eruptions on the Island of Nisyros). High numbers of glass shards make the tephra layers discernible with sharp tops and bases in most of the cores; however, some are disseminated in fine mud. For example, Unit E contains an ash layer, disseminated in mud in cores MAR03-25 and MAR03-02, which is correlated with the X1 tephra, most likely derived from the Aeolian Islands, Italy (Aksu et al., 2008).

Sapropel units B, D, F, and H are distinguished from overlying/underlying units by their darker olive gray colour (5Y4/1, 5Y3/2, 5Y4/2, 5Y5/2, 5Y2/2, 5Y2/1). They are composed of sharp-based colour-banded clayey mud overprinted by sharp-walled branching millimetre-diameter burrows identified as *Chondrites*. The organic carbon contents range from 1% to 12.65%.

### 3.2. Age models

The chronostratigraphy of the cores was established using a number of age control points that permit a depth-to-age conversion with the assumption that the sedimentation rate was constant between dated levels. The age control points consist of well constrained top/bottom ages of unit B (sapropel S1); tephra layers Z2, Y2, and Y5; and control points determined by curve matching of the oxygen isotope curves for each core with the global oxygen isotope curve of Lisiecki and Raymo (2005). The Nisyros ash (Figure 3) was not used because the age proposed by Aksu et al. (2008) for this tephra is now in question (Margari et al., 2007) and it is likely older than Aksu et al. (2008) reported, perhaps 54–58 ka rather than 42–44 ka (V. Margari and D. Pyle, pers. comm. 2011). Unit B is correlated with the most recent sapropel S1 due to its consistent stratigraphic position throughout the cores, situated between the ash layers Z2 and Y2, and its occurrence within MIS 1. Its top/bottom ages (6600 and 9900 $^{14}$C yr BP, respectively; Table 3) are well constrained by other researchers; calibrated dates based on these $^{14}$C ages and a reservoir age of 557 yr (Facorellis et al., 1998) are used as age control points. The oldest sediment recovered in the cores (unit I) was deposited ~130 ka at the transition from MIS 6 to MIS 5 (Table 3).

The interpolated basal ages of organic-rich Units D, F, and H are 83.2–80.4 ka, 106.4–105.8 ka, and 128.6–128.4 ka, respectively. These calculated ages coincide with the substages of MIS 5 and are in good agreement with the previously published ages of sapropels S3, S4, and S5 developed during marine isotopic stages 5a, 5c, and 5e in the eastern Mediterranean Sea (Rossignol-Strick, 1985; Emeis et al., 2003).

The mean sedimentation rates for cores MAR03-28, MAR03-03, MAR03-02, MAR03-25, and MAR03-27 are 6.4 cm/ka, 4.7 cm/ka, 9.5 cm/ka, 6.0 cm/ka, and 11.5 cm/ka, respectively (Table 3). Considering the 10-cm sampling interval, calculated accumulation rates imply a temporal sample-to-sample resolution for these cores of 1560 yr, 2125 yr, 1050 yr, 1665 yr, and 870 yr, respectively.

### 3.3. Planktonic foraminifera

All samples examined for foraminifera include variable amounts of aragonitic pteropods, which suggest that the foraminifera in the Aegean Sea cores sustained little to no dissolution and that the observed fauna in the cores likely

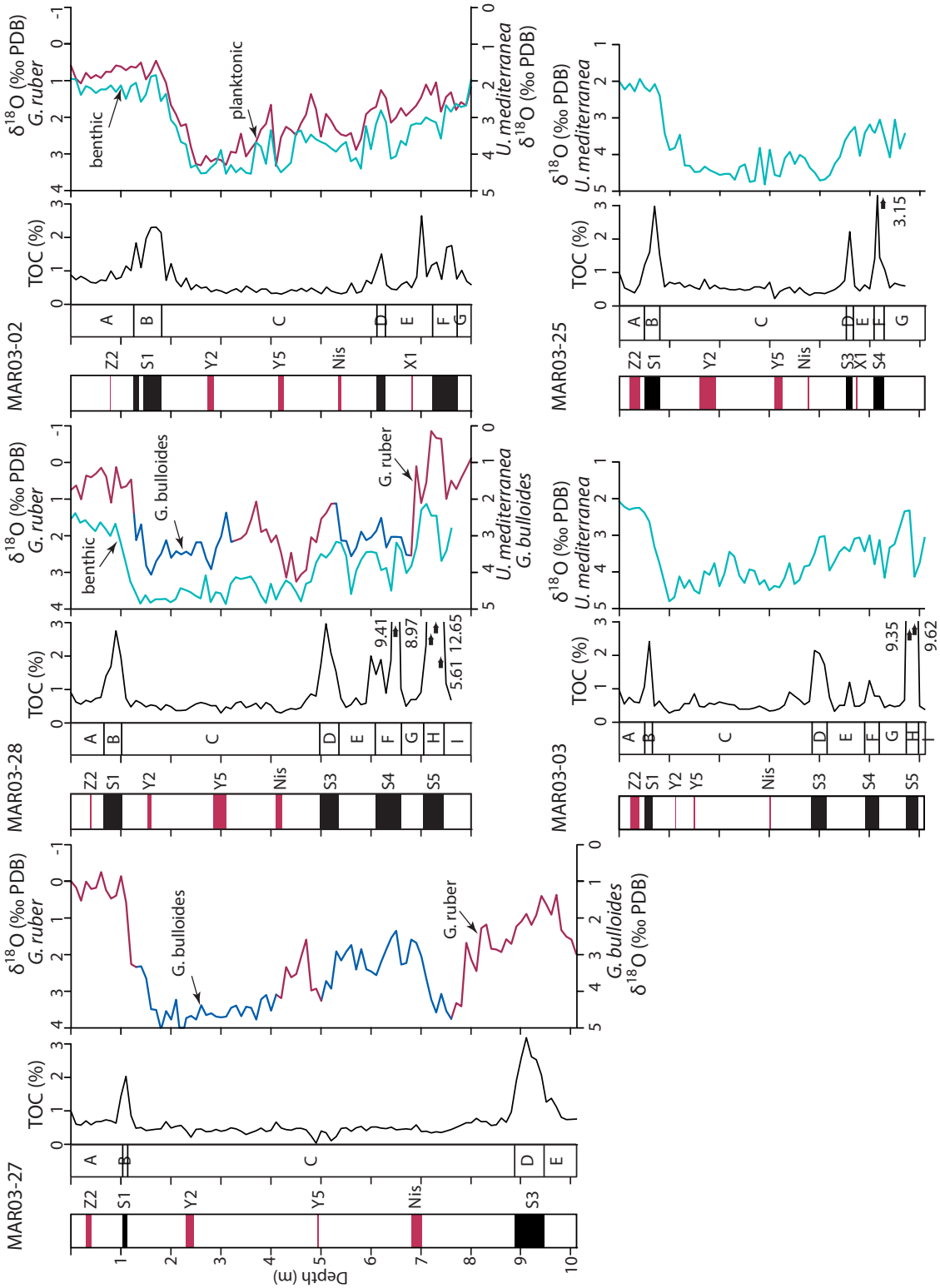


**Figure 2.** Downcore plots showing the lithostratigraphic units (A through I), total organic carbon (TOC) contents and the variations in oxygen isotope values ($\delta^{18}O$) in the Aegean Sea cores. Red and blue lines are the $\delta^{18}O$ values in planktonic foraminifera *G. ruber* and *G. bulloides*, respectively, aquamarine lines are the $\delta^{18}O$ values in benthic foraminifera *U. mediterranea*. MIS = marine isotopic stages. Black fills = sapropels, red fills = volcanic ash layers (from Aksu et al., 2008). Core locations are shown in Figure 1.

**Table 3.** Calculated ages of sapropels S3, S4, and S5.

| | | S3 | S4 | S5 |
|---|---|---|---|---|
| MAR03-02 | Onset | 82,800 | 106,400 | ---- |
| | End | 76,600 | 94,400 | ---- |
| MAR03-03 | Onset | 83,200 | 105,800 | 128,600 |
| | End | 72,600 | 100,600 | 123,600 |
| MAR03-25 | Onset | 81,600 | 105,600 | ---- |
| | End | 76,800 | 97,800 | ---- |
| MAR03-27 | Onset | 80,400 | ---- | ---- |
| | End | 74,000 | ---- | ---- |
| MAR03-28 | Onset | 80,600 | 105,800 | 128,400 |
| | End | 70,800 | 96,200 | 121,000 |

represent the surface water assemblages near each core site at the time of deposition. In basins where the foraminiferal lysocline is deep and bottom waters are not corrosive, the living planktonic foraminiferal assemblages in surface waters are well represented in the bottom sediments (e.g., Schiebel et al., 2004, Retaileau et al., 2012).

### 3.3.1. Downcore distribution of planktonic foraminiferal ecozones

Seventeen planktonic foraminiferal species were identified. The dominant species that constitute >85% of the total assemblage are *N. pachyderma* dextral (hereafter denoted by d), *G. bulloides*, *G. ruber* (white), *Turborotalita quinqueloba*, *G. inflata*, *Globigerinita glutinata*, *G. scitula*, *Orbulina universa*, and *N. dutertrei*. The remaining eight species (*Globigerinella aequilateralis*, *Globigerinoides sacculifer*, *G. ruber* (pink), *Globigerinella calida*, *Globorotalia crassaformis*, *Globigerinoides rubescens*, *Globigerinoides tenellus*, and *N. pachyderma* (sinistral; hereafter denoted by s)) display sporadic appearances not exceeding 5% of the total fauna. Tropical taxa (i.e. *G. aequilateralis*, *G. sacculifer*, *G. ruber* (pink), *G. calida*, *G. crassaformis*, *G. rubescens*, and *G. tenellus*) occur together and are only present in low abundances; they are plotted together as the parameter 'warm'.

The planktonic foraminiferal data matrix was used to perform a 'mean-within cluster sum of squares' cluster analysis, CONISS (CONstrained Incremental Sums of Squares; Grimm, 1987). The final clusters were delineated by drawing a straight line at the value 0.04 on the distance/

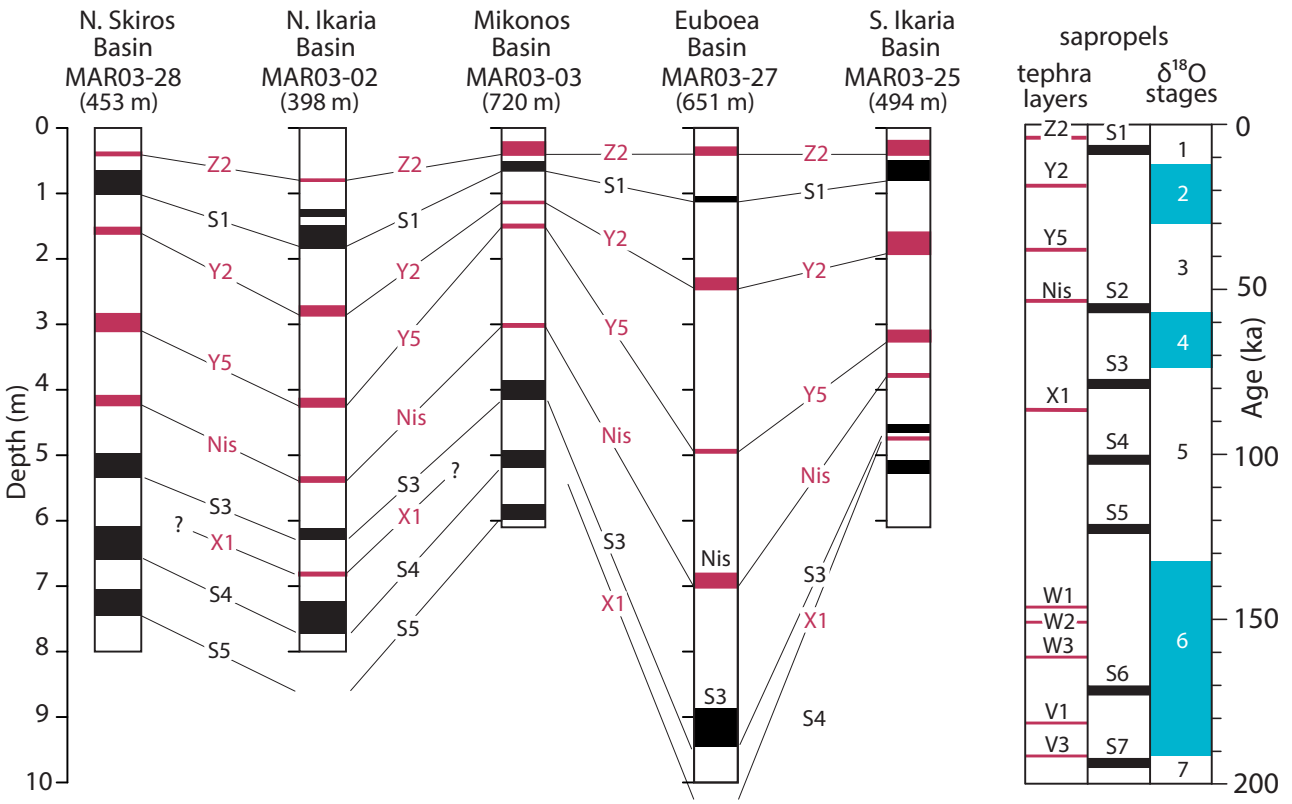


**Figure 3.** Correlation of ash layers (red) and lithostratigraphic units across the Aegean Sea cores. Ash layers Z2, Y2, Y5, Nis, X1 (red fills) are from Aksu et al. (2008). Sapropels are shown as black fills with S1, S3, S4, and S5 designations. Global oxygen isotopic stage boundaries are from Lisiecki and Raymo (2005). Core locations are shown in Figure 1.

similarity measure of each dendrogram. Species that are associated (i.e. that cluster) in the distance/similarity range 0.00–0.04 are recognized as 'planktonic foraminiferal ecozones', hereafter referred to as 'ecozones' I though IV. Ecozone IV is further subdivided into six subecozones (Figures 4–8). In this study, the ecozones are arranged stratigraphically, through time, without downcore repetition.

The downcore variations in the proportions of individual planktonic foraminifera generally show distinctive distribution patterns broadly correlated with the ecozones identified using the cluster analysis results, suggesting that the large-scale climatic and oceanographic conditions across the Aegean Sea during the Late Quaternary are faithfully recorded by the planktonic foraminiferal data (e.g., Schiebel et al., 2004).

Ecozone I (0–13 ka) is characterized by high abundances of *G. ruber* and *G. bulloides* (>85% of the total foraminiferal assemblage), the consistent presence of the tropical species, and episodic appearances of *N. pachyderma*(s), *G. inflata*, and *O. universa* (Figures 4–8). *G. ruber* exhibits a higher amplitude variation, particularly within the upper half of the ecozone.

Ecozone II (~40–13 ka) is characterized by the dominance of *N. pachyderma* (d), low percentages of *G. ruber* and *G. bulloides*, and the absence of *G. inflata*. *N. pachyderma* (d) generally increases upward; for example, from 43% to 81% in core MAR03-28 and from 27% to 51% in core MAR03-25 (Figures 4–8). *G. ruber* shows low percentages (<10%) and, particularly in the most northerly core MAR03-28, abundances do not exceed 5% in the middle portion of the ecozone. *T. quinqueloba* is consistently present in all cores, ranging from 1% to ~30%. *G. glutinata* ranges between 1% and 22%, whereas *G. scitula*, *N. pachyderma* (s), and *N. dutertrei* are generally <10%.

Ecozone III (~40–60 ka) is characterized by the continuous presence of *G. inflata* and lower abundance variations of *N. pachyderma* (d) relative to Ecozone II (Figures 4–8). *G. ruber* and *G. bulloides* exhibit moderate frequency and high amplitude variations throughout the cores, ranging generally between 10% and 40%. *T. quinqueloba* shows a negative excursion similar to *N. pachyderma* (d), attaining high percentages of 20%–25% at the base and top of the ecozone and decreasing to 4%–11% in the middle. Ecozone III is marked at its base by a mostly sharp to locally gradual downward disappearance of *G. inflata* (Figures 4–8).

Ecozone IV (>60 ka) is characterized by large amplitude variations in the abundances of *N. pachyderma* (d), *G. ruber*, and *G. bulloides* and episodic appearances of *N. dutertrei* (Figures 4–8). These variations are used to subdivide the ecozone into six subecozones, IVa–IVf.

Subecozone IVa is characterized by a dominance of *N. pachyderma* (d), downward increase in *N. dutertrei*, and consistent upward increase in *G. ruber* (Figures 4–8). *G. bulloides* generally varies from 12% to 35% and *T. quinqueloba* and *G. inflata* generally show consistent abundances ranging between ~5% and 30% and between 3% and 38%, respectively.

Subecozone IVb is characterized by a dominance of *G. ruber* (38%–58%) and *G. bulloides* (13%–25%), near disappearance of *N. dutertrei*, and general upward increasing trend of *G. inflata* (~6%–21%; Figures 4–8). *N. pachyderma* (d) displays large amplitude negative inflections with values ranging between 33% and 65%.

Subecozone IVc is characterized by high abundances of *N. pachyderma* (d) (~30%–75%) and very low abundances of *G. ruber* (~4%), *G. bulloides* (~7%), and *N. dutertrei* (8%) (Figures 4–8). Generally, the maximum abundances of *N. dutertrei* coincide with the minimum abundances of *G. inflata*.

Subecozone IVd is characterized by low *N. pachyderma* (d) percentages, notably increased abundances of *G. ruber* and *G. bulloides*, and the disappearance of *T. quinqueloba* and *N. dutertrei* (Figures 4–8).

Subecozone IVe coincides with high abundances of *N. pachyderma* (d) (65%–70% in only cores MAR03-03 and MAR03-28; Figures 4 and 7). *G. ruber* and *G. bulloides* exhibit negative excursions with abundances of 20%–40%. *N. dutertrei* and *O. universa* are consistently present across the subecozone, generally showing abundances of 6%–9% (Figures 4 and 7).

Subecozone IVf covers the lowermost portions of cores MAR03-03 and MAR03-28 (Figures 4 and 7). *G. bulloides* ranges between ~20% and 40%. *N. pachyderma* (d) ranges between >20% and <60%.

### 3.4. Oxygen isotopes

The age-converted stacked $\delta^{18}O$ curves for planktonic and benthic foraminifera illustrate that there are consistent variations in the oxygen isotopic composition of the Aegean Sea water masses since 130 ka. Moderate to large amplitude excursions correspond to glacial and interglacial stages (Figure 9). Abrupt depletions in the $\delta^{18}O$ values characterize the upper segments of all cores with changes of as much as 4‰ at the most recent glacial–interglacial transition (i.e. marine isotopic stage MIS 2/1 boundary; Figure 9). Planktonic foraminiferal $\delta^{18}O$ values are notably heavier during glacial periods (i.e. 2.8‰–3.2‰ in MIS 2 and MIS 4), suggesting cooler and possibly more saline conditions. Similar to the trends observed in global oxygen isotopic data (e.g., Lisiecki and Raymo, 2005) downcore variations in oxygen isotope values in the Aegean Sea cores show that the interglacial–glacial transitions are more gradual than the glacial–interglacial transitions. The depleted $\delta^{18}O$ values during MIS 1 and MIS 5 show clear

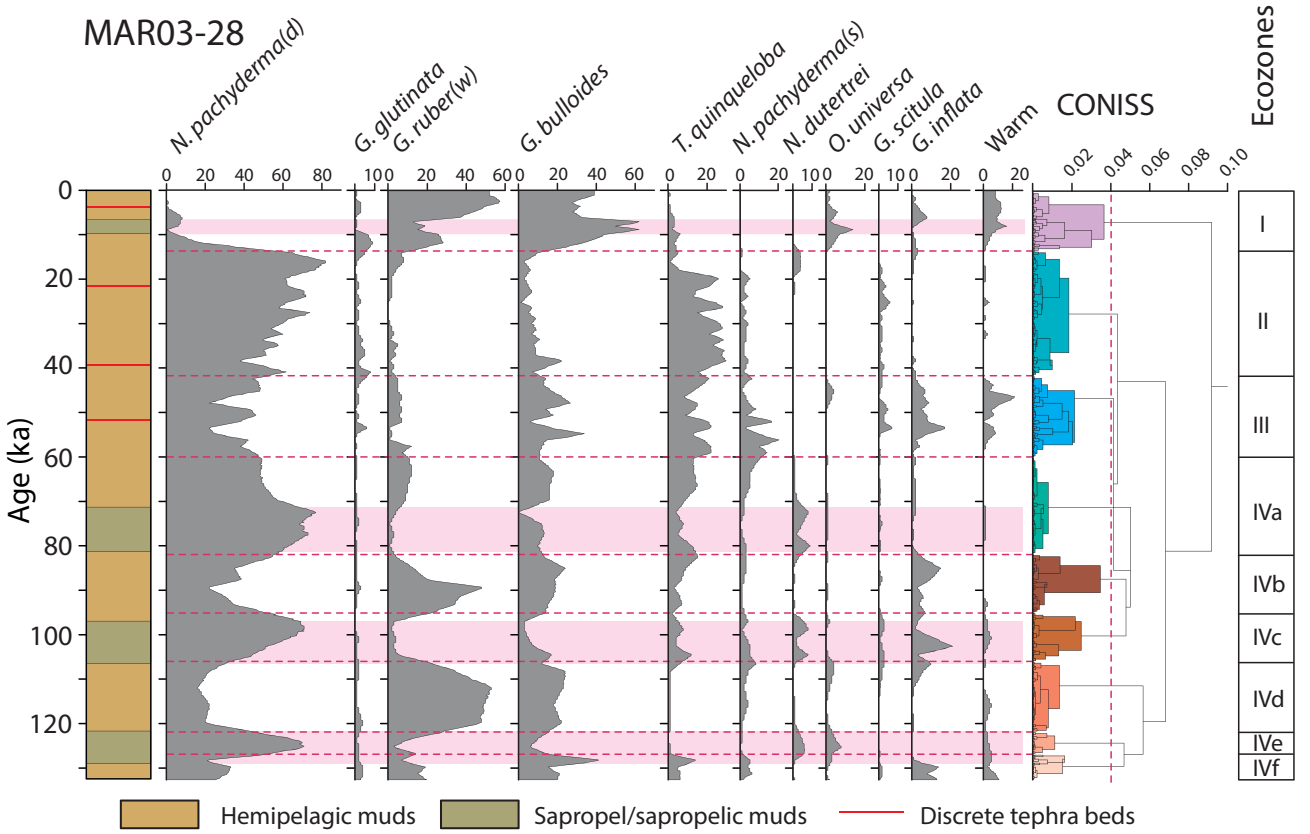


**Figure 4.** Downcore assemblage distributions of planktonic foraminifera in core MAR03-28. The right column shows the results of cluster analysis and the resulting ecozones. Core location is shown in Figure 1.

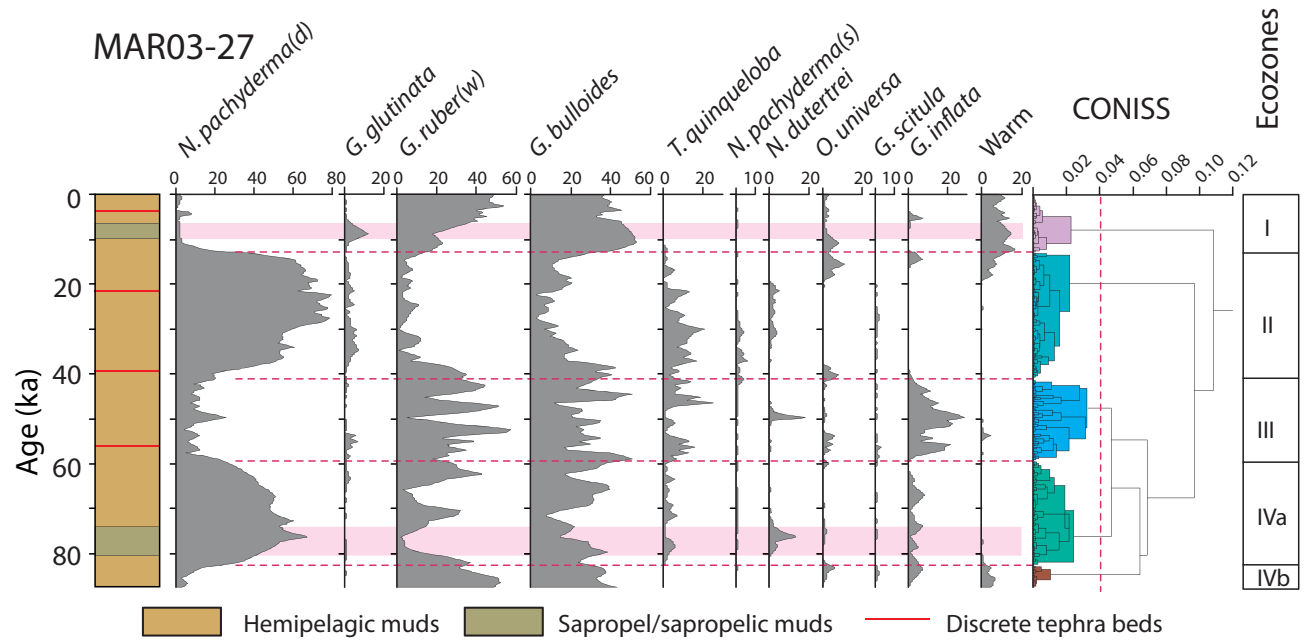


**Figure 5.** Downcore assemblage distributions of planktonic foraminifera in core MAR03-02. The right column shows the results of cluster analysis and the resulting ecozones. Core location is shown in Figure 1.

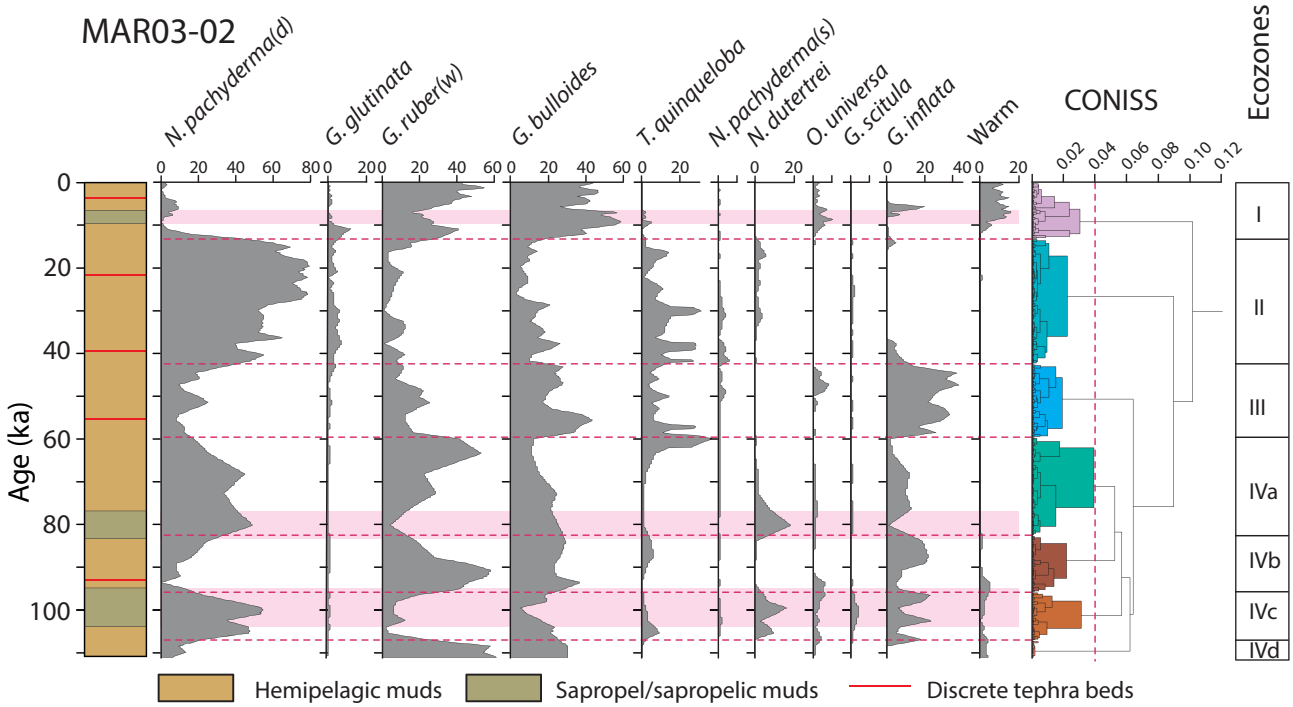


**Figure 6.** Downcore assemblage distributions of planktonic foraminifera in core MAR03-03. The right column shows the results of cluster analysis and the resulting ecozones. Core location is shown in Figure 1.

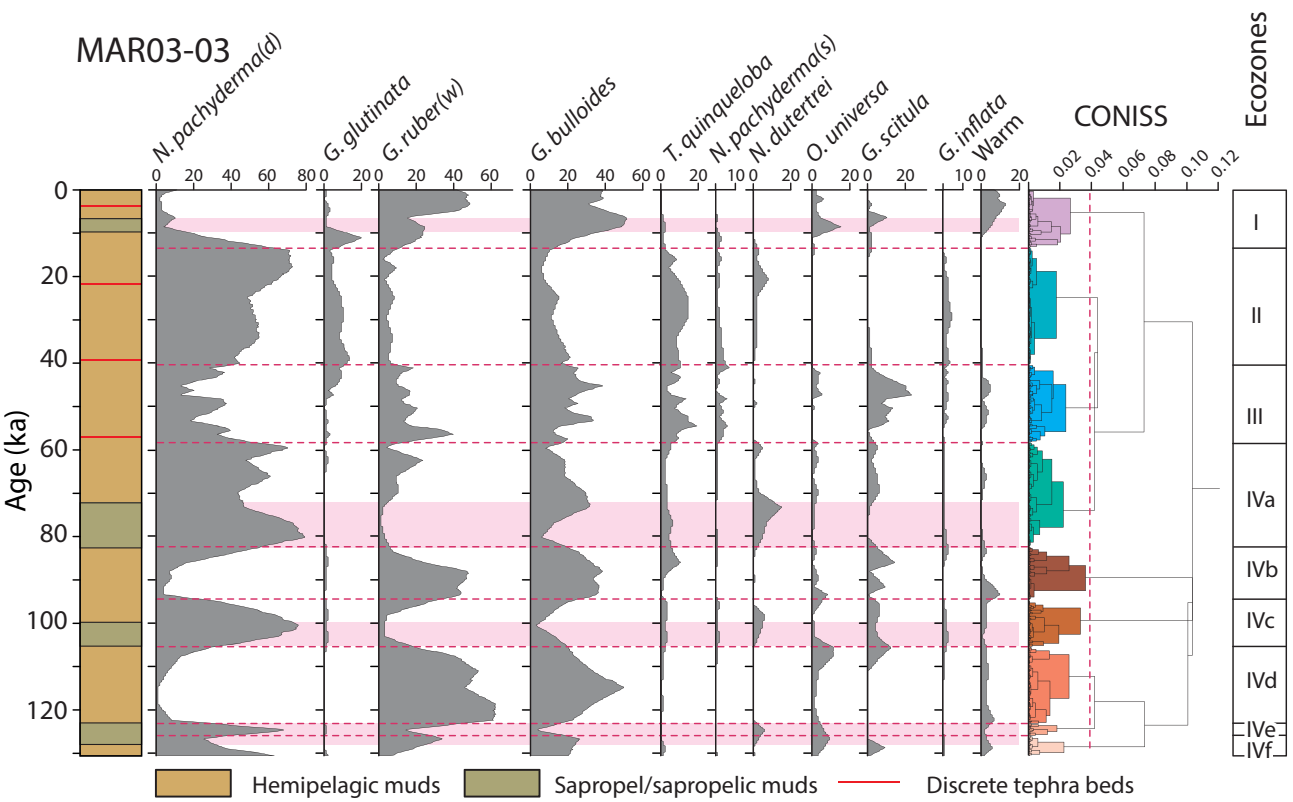


**Figure 7.** Downcore assemblage distributions of planktonic foraminifera in core MAR03-03. The right column shows the results of cluster analysis and the resulting ecozones. Core location is shown in Figure 1.

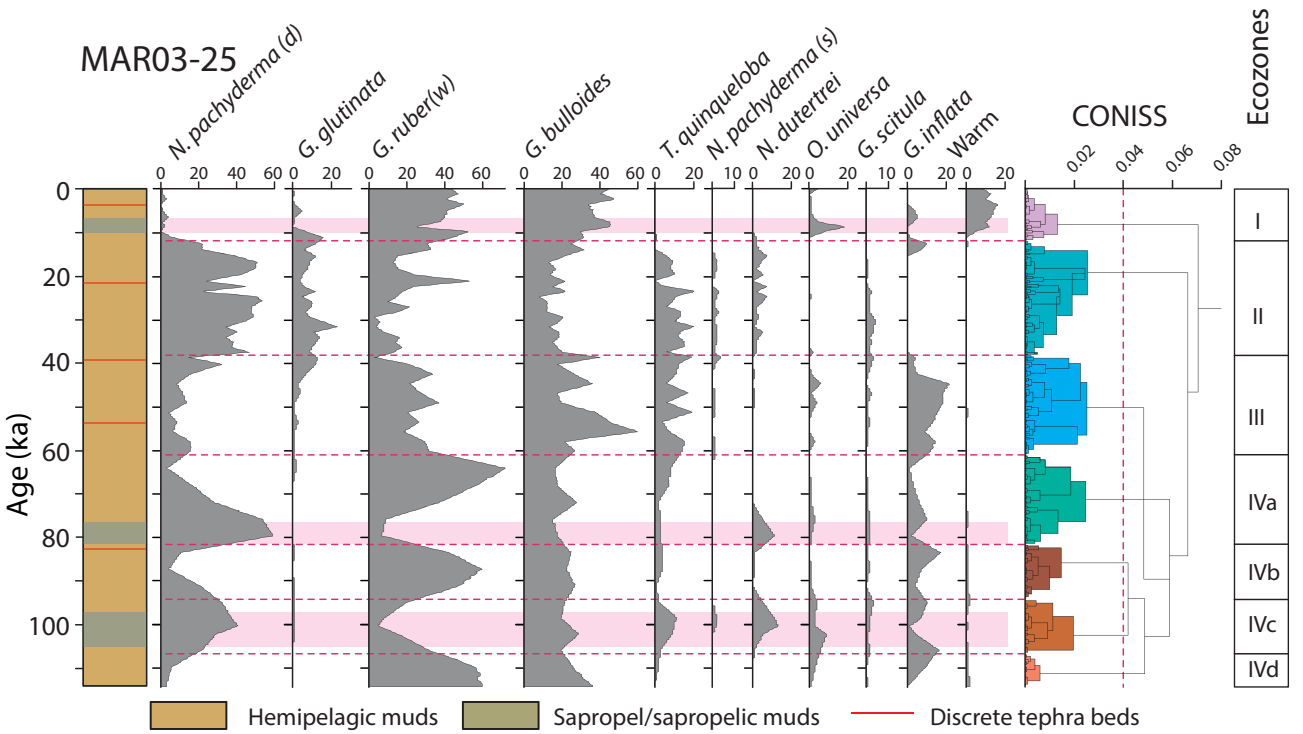


**Figure 8.** Downcore assemblage distributions of planktonic foraminifera in core MAR03-25. The right column shows the results of cluster analysis and the resulting ecozones. Core location is shown in Figure 1.

association with times of sapropel deposition. The data show that depletions are strongest during and immediately following the accumulation of sapropels S1 and S5, ranging from 0.6‰ to 0.9‰ in *U. mediterranea* and from 0.3‰ to –0.6‰ in *G. ruber* and *G. bulloides*. In sapropels S3 and S4, $\delta^{18}O$ values show similar yet modest variations changing on average by between 1.4‰ and 1.8‰ relative to adjacent units. In cores MAR03-28 and MAR03-02, the magnitudes of the depletions and enrichments in the planktonic and benthic $\delta^{18}O$ values are similar to one another (Figure 9).

### 3.5. Carbon isotopes

Carbon isotope values obtained from planktonic and benthic foraminifera generally range between 0.0‰ and 1.5‰ with conspicuous depletions (–0.5‰ and –1.0‰) in the uppermost parts of cores MAR03-25 and MAR03-02, coinciding with sapropel S1 (Figure 10). Consecutive and large amplitude excursions of as much as 1.0‰ are recognized in the lower half of the cores (encompassing MIS 5), where sapropel layers S3, S4, and S5 generally correlate with the $\delta^{13}C$ depletions.

### 3.6. Sea surface temperature (SST) and sea surface salinity (SSS)

Based on transfer-function calculations, high amplitude temperature and salinity variations of ~8–12 °C and 1.5 psu occurred during MIS 5 and the transition from MIS 2 to MIS 1 (Figure 11). Fluctuations during MIS 5 are notably larger in cores MAR03-28 and MAR03-03 than those in cores MAR03-25 and MAR03-02. Within the upper half of sapropel S5 in cores MAR03-28 and MAR03-03, SST and SSS values show a progressive upward increase into the overlying nonsapropel unit G, changing from 14 °C to 23 °C and from 36.7 psu to 38.3 psu. In core MAR03-28, SST and SSS estimates are around 16 °C and 37.3 psu at the top and bottom of sapropel S5 and are lower (13.6 °C and 35.2 psu) immediately above the middle of the sapropel at around 125 ka (Figure 11).

Toward and well into the time of accumulation of sapropel S4, temperature and salinity decreased at all core sites and minima were attained mainly close to the sapropel top (except in core MAR03-02). At core sites MAR03-28 (most northerly) and MAR03-03, the magnitude of these drops was as much as 10 °C and 1.8 psu. During the deposition of sapropel S4, surface waters were warmer and more saline at southernmost core site MAR03-25 than at other sites, changing between 21 °C and 37.9 psu at the base of S4 to 19 °C and 36.7 psu at its top. Minimum temperature and salinity values of 11.8 °C and 36.5 psu were calculated within the upper half of sapropel S4 at the most northerly core site MAR03-28, becoming 16–17 °C and 37.6 psu at the bottom and top of S4 (Figure 11). In core MAR03-02, SST shows a continuous upward increase from 17 °C to 21.8 °C across S4 with relatively

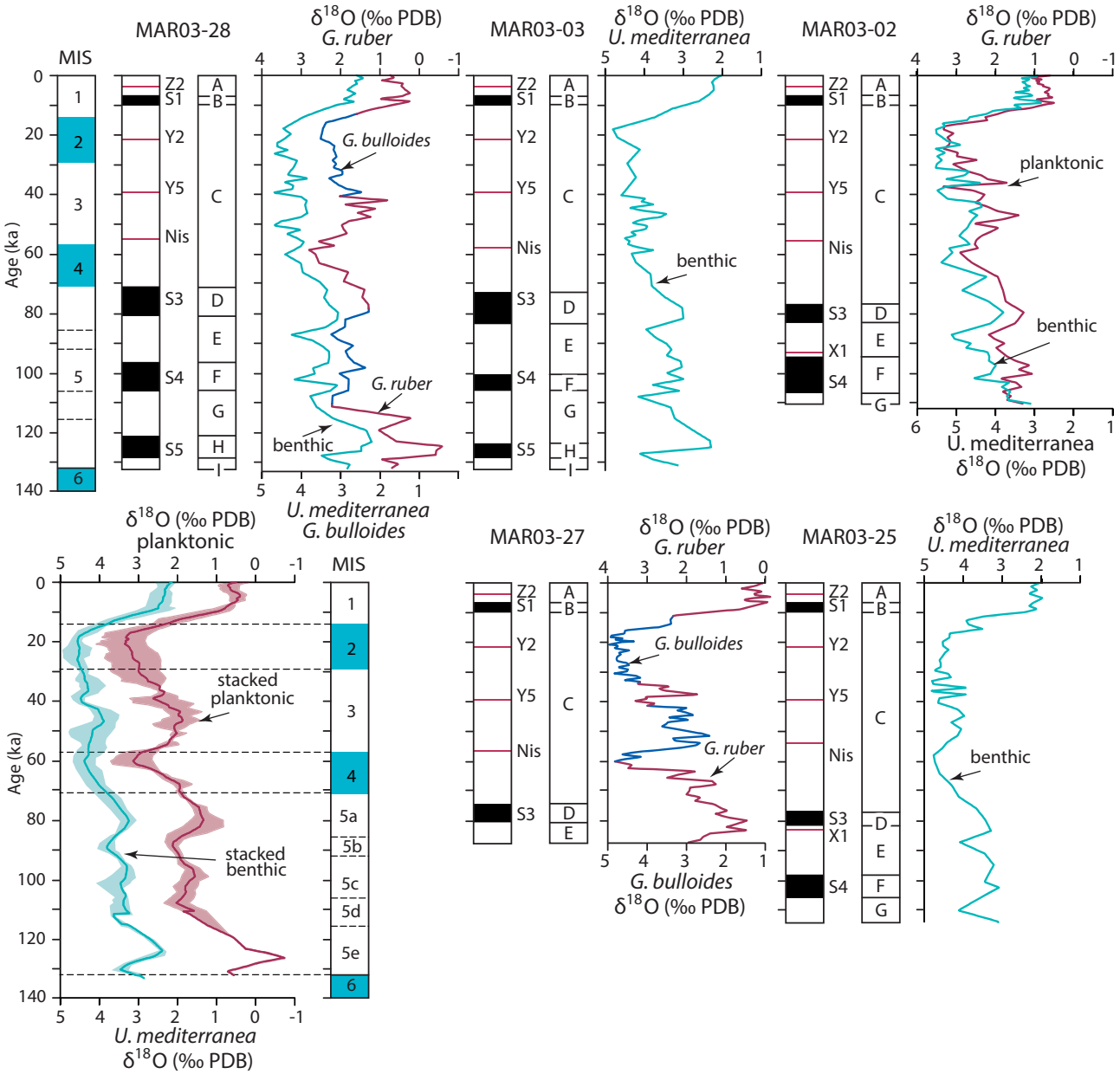


**Figure 9.** Generalized downcore variations of oxygen isotopic compositions in planktonic foraminifera *G. ruber* (red) and *G. bulloides* (blue) and benthic foraminifera *U. mediterranea* in the Aegean Sea during the last ca. 130 ka. Graph on the lower left is the stacked planktonic and benthic oxygen isotopic compositions (red and aquamarine shaded envelopes, respectively). Stacking is achieved by averaging the age-converted benthic and planktonic oxygen isotopic values in cores MAR03-02, MAR03-03, MAR03-25, MAR03-27, and MAR03-28. Heavy aquamarine (benthic) and red (planktonic) lines are the averaged values. Core locations are shown in Figure 1.

constant surface salinity (~37 psu). Successive SST and SSS increases continued above S4 until 86 ka at core site MAR03-25 and until around 91 ka at the remaining four core sites, reaching temperatures and salinities ranging mainly between 21.5 and 22.5 °C and 38 and 38.6 psu.

Toward the onset of sapropel S3, SST and SSS show a persistent drop until around 82 ka, reaching minimum values of 18–18.5 °C and 37.3–37.1 psu at core sites MAR03-25 and MAR03-02 and 12–14 °C and 36.4–36.1 psu in cores MAR03-03 and MAR03-28 (Figure 11). The SST and SSS values exhibit small variations during the deposition of sapropel S3, ranging from 10 °C to 13 °C and from 36.4 psu to 37.1 psu at northerly core sites MAR03-28 and MAR03-27 and from 16 °C to 18 °C and from 36.7 psu to 37.3 psu at core sites MAR03-25, MAR03-03, and MAR03-02. Until 46 ka, SST and

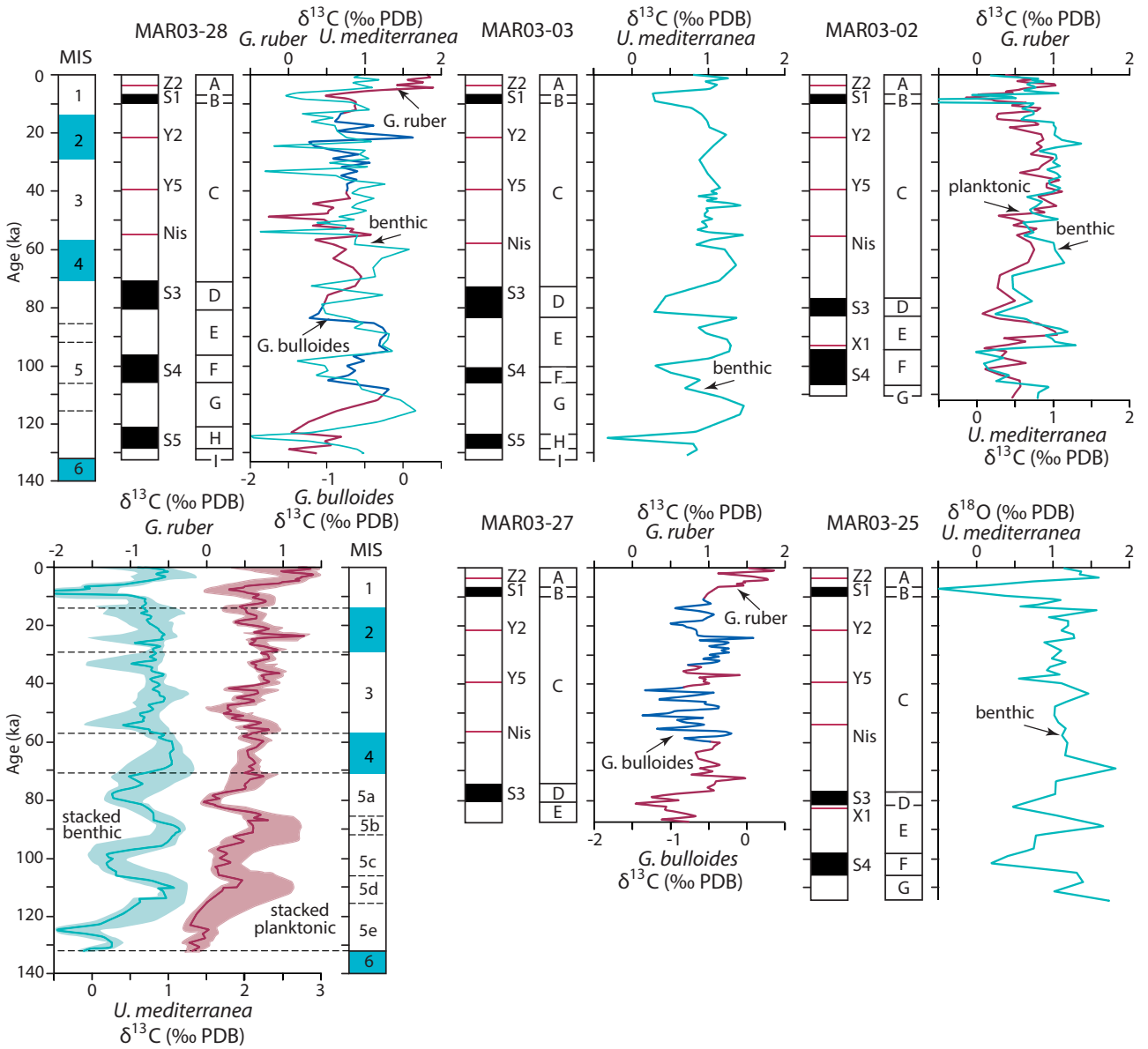


**Figure 10.** Generalized downcore variations of carbon isotopic compositions in planktonic foraminifera *G. ruber* (red) and *G. bulloides* (blue) and benthic foraminifera *U. mediterranea* in the Aegean Sea during the last ca. 130 ka. Graph on the lower left is the stacked planktonic and benthic carbon isotopic compositions (red and aquamarine shaded envelopes, respectively). Stacking is achieved by averaging the age-converted benthic and planktonic carbon isotopic values in cores MAR03-02, MAR03-03, MAR03-25, MAR03-27, and MAR03-28. Heavy aquamarine (benthic) and red (planktonic) lines are the averaged values. Core locations are shown in Figure 1.

SSS gradually increased and generally show 2–3 °C and 1 psu variations, ranging from 11.5 to 13.5 °C and from 36.5 to 37.2 psu at the most northerly core site MAR03-28 and from 18–20.2 °C and 37–38.1 psu to 19.2–22 °C and 37.2–38.2 psu at more southerly sites MAR03-02 and MAR03-25, respectively (Figure 11). In core MAR03-27, relatively extended periods of temperature and salinity increases are observed until 36 ka. This relatively warm interval is followed by a continuous drop in surface water temperatures and salinities, indicating the gradual change from interglacial to glacial conditions associated with the transition from MIS 3 to MIS 2. At core sites MAR03-02, MAR03-03, and MAR03-28, glacial conditions were attained rather more rapidly (at ~39 ka) than at core sites MAR03-27 and MAR03-25. The former three core sites show 4–8 °C and 0.4–1.0 psu drops attaining minimum temperatures of 11–12 °C at core sites MAR03-03 and MAR03-02 and 8–10 °C at the most northern core site

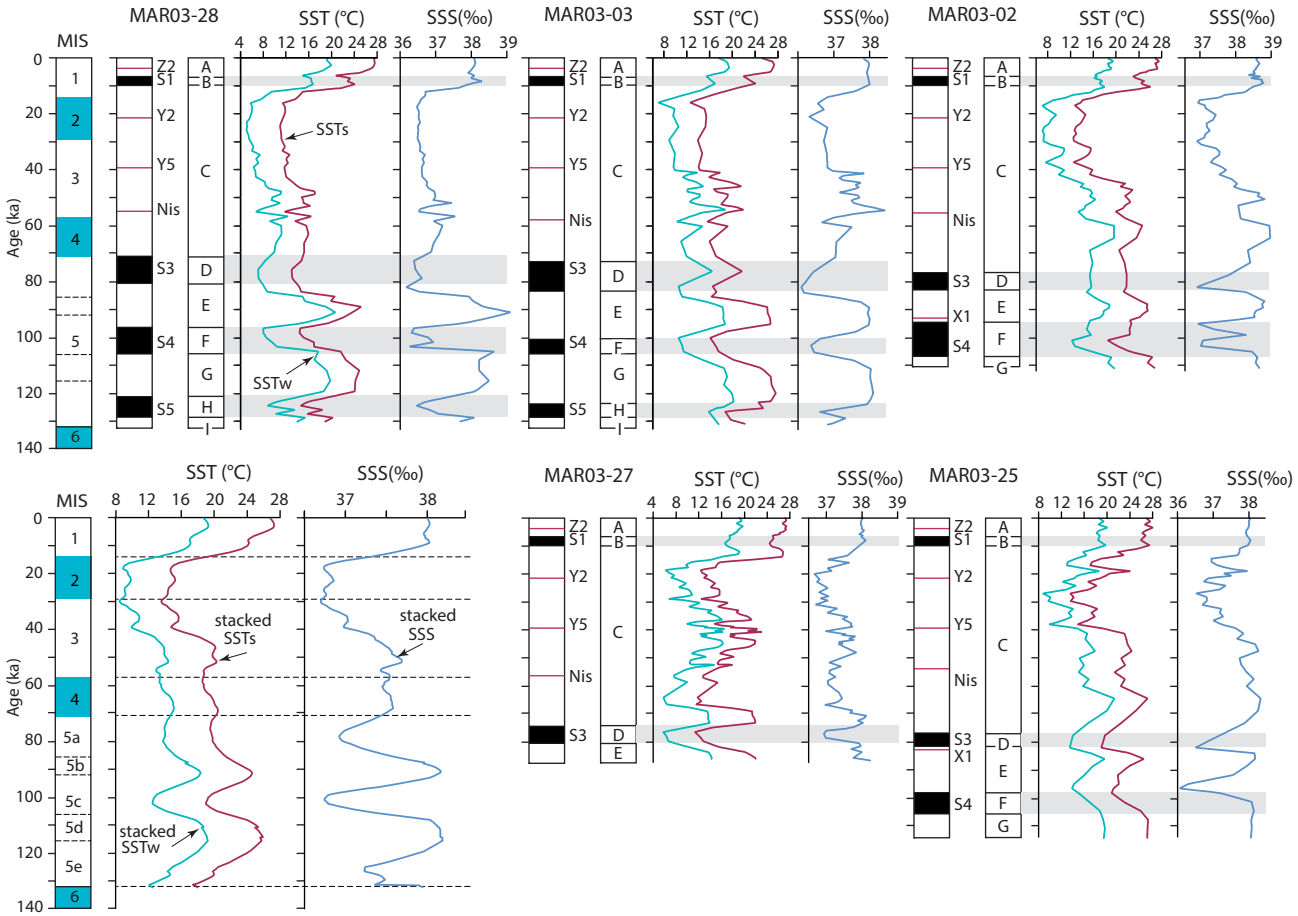


**Figure 11.** Sea surface temperature (SST) and sea surface salinity (SSS) variations of five cores. Horizontal grey bars highlight the sapropel intervals. MIS = marine isotopic stages. Black fills = sapropels, red fills = volcanic ash layers (from Aksu et al., 2008). Core locations are shown in Figure 1.

MAR03-28 (Figure 11). These glacial temperature and salinity values were maintained until 18 ka. Between 18 ka and core tops (Recent), continuous and very high amplitude temperature and salinity increases are observed at all core sites, associated with the transition from MIS 2 to MIS 1. The SST values show 1–2 °C temperature decreases immediately below the most recent sapropel S1. Cooler and less saline surface waters lingered during the deposition of sapropel S1 and then the sea surface warmed up to its previous state following the cessation of sapropel formation. The SST values continued to rise toward the core tops, becoming ~2–3 °C warmer since 5 ka (Figure 11).

### 3.7. SST from Mg/Ca ratios

It has been argued that SST values in geographically confined seas, such as the Aegean Sea, cannot be reliably estimated because of the high amplitude fluctuations in temperature, salinity, and productivity in such enclosed basins (e.g., Sperling et al., 2003). A solution is to apply more than one method to determine seawater paleotemperature, in the belief that coincident estimates from independent methods are more likely to be correct. Foraminiferal transfer functions have provided one set of constraints (Figure 11). The Mg/Ca ratio in foraminiferal calcite provides a second SST estimate (Lea et al., 2000; Dekens et al., 2002; Rosenthal and Lohmann, 2002; Anand et al., 2003).

In the Aegean Sea cores, the SST values obtained from Mg/Ca ratios agree closely with summer SST values calculated using transfer functions (Figure 12). Mg/Ca ratios were obtained from *G. ruber*, which is a warm-water indicator and has been used to estimate summer seawater paleotemperatures. Both SST estimators support the presence of cooler surface waters (at least during summer) during accumulation of sapropels S5, S4, S3, and S1 (Figures 11 and 12). The presence of small percentages of *N. pachyderma* (s) during these intervals supports this interpretation (Figures 4–8).

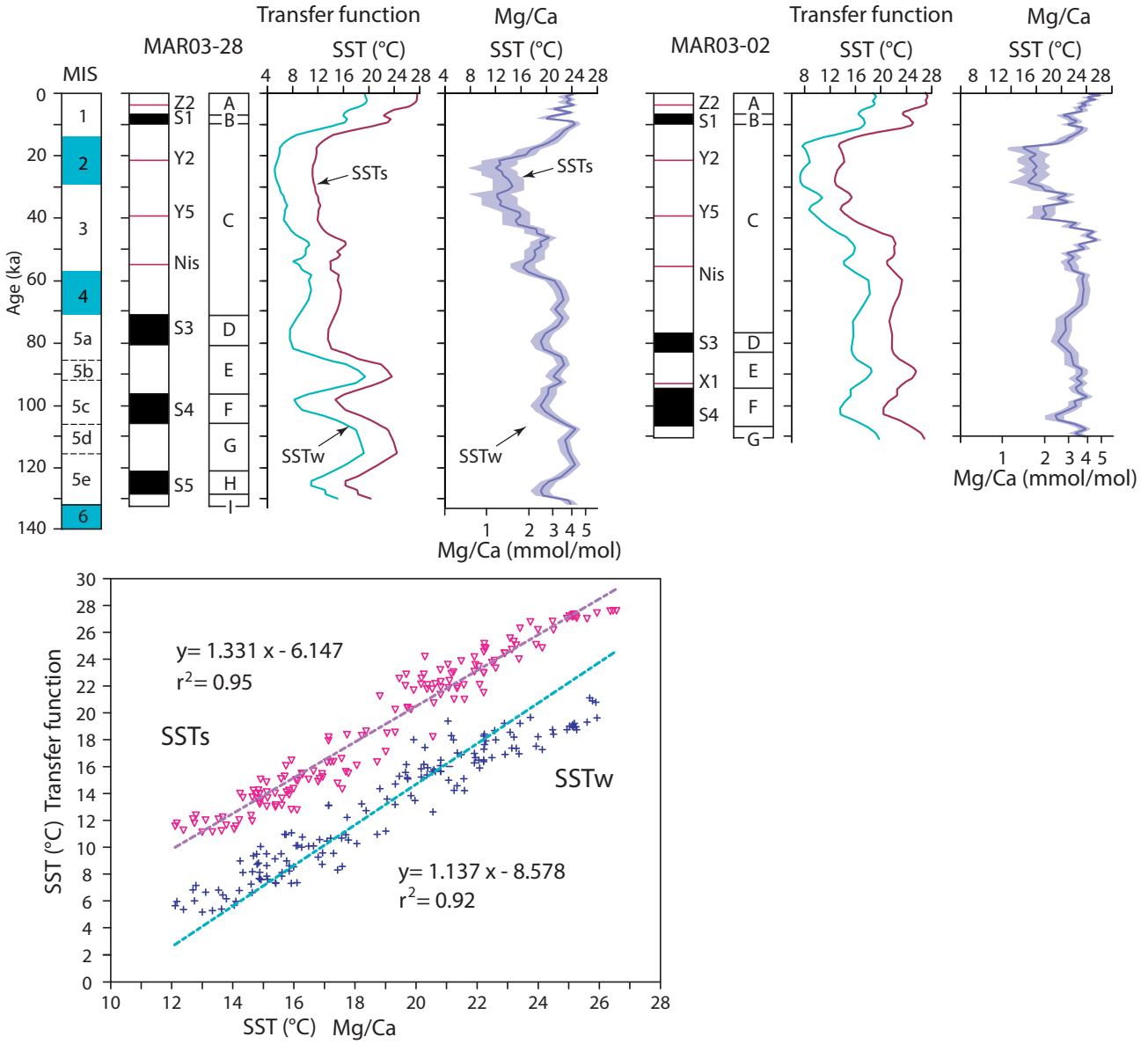


**Figure 12.** Comparison of the sea surface temperatures calculated using the planktonic foraminiferal transfer functions and Mg/Ca in cores MAR03-28 and MAR03-02. Grey and yellow envelopes show the calculated values with error bars. Core locations are shown in Figure 1.

Transfer function temperature variations during transitions from interstadials to stadials of MIS 5 show large amplitude fluctuations of 9–10 °C in cores MAR03-28 and MAR03-03, whereas in cores MAR03-02 and MAR03-25 these variations are smaller at 3–5 °C. The fluctuations are similar to those reported by van der Meer et al. (2007). However, temperature fluctuations of 9–10 °C exceed what would be expected for oxygen isotopic changes of ~1.2‰ during transitions (e.g., MIS 5d/5c), assuming that the isotopic ratio changes by ~0.2‰ $\delta^{18}O$/°C (e.g., Emeis et al., 2000). The percentage of *N. pachyderma* (d) tests (subpolar species) in cores MAR03-28 and MAR03-03 is at least 20% higher than in other cores, and it is these abundance peaks that account for the higher amplitude temperature variations (~10 °C) in these cores. These large shifts might be overestimates and the smaller fluctuations based on Mg/Ca ratios (~4 °C; Figure 12) are thought to be more accurate.

It is interesting that the paleotemperature estimates based on both faunal and Mg/Ca data indicate cooling during the sapropel deposition during MIS 5. This cooling trend, particularly the one that is associated with the

MIS 5e, is challenging because during this period the summer insolation values were at their maximum (Berger, 1978; Berger et al., 2005, 2006). There are two possible explanations for the observed SST and SSS trends: (i) the faunal paleotemperature results are heavily biased by increases in *N. pachyderma* (d) and/or by variations in sea surface salinities, leading to low reliability in the trends, or (ii) these trends are correct and the landlocked Aegean Sea indeed experienced cooling during the deposition of the MIS 5 sapropels. As a caveat, freshwater/nutrient input from both the northern and eastern rivers draining into the region, as well as freshwater influx from the south associated with intensified African monsoons, might have altered the salinity structure of the Aegean Sea, thus potentially influencing the Mg/Ca ratio in foraminiferal calcite (Ferguson et al., 2008). However, decreases in sea surface temperatures of 2 °C for sapropel S5 and 6 °C for S4 determined for the eastern Mediterranean Sea core MD84-641 collected off the Nile River (Kallel et al., 2000) are consistent with our results and suggest that the faunal and Mg/Ca paleotemperatures reported here are correct.

## 4. Discussion

### 4.1. Significance of downcore distribution of G. bulloides

*G. bulloides* is one of the more dominant planktonic foraminiferal species in the Mediterranean region, including the Aegean and Adriatic seas. This species tolerates a wide spectrum of temperatures and inhabits a broad depth range, generally in the upper 100–200 m of the water column. It is an indicator of eutrophic waters and upwelling (Rohling et al., 1993, 1997; Zaric et al., 2005).

During sapropel S1 deposition, higher abundances of both *G. bulloides* and *G. ruber* (white) are observed throughout the Aegean and the Adriatic seas and are ascribed to either elevated nutrient concentrations in surface waters due to enhanced river runoff or lower oxygen content within the photic zone as a result of phyto and zooplankton blooms (Rohling et al., 1993; Principato et al., 2003; Geraga et al., 2005). The covariation of *G. bulloides* and *G. ruber* (white) during sapropel S1 deposition is supported by our work (Figures 4–8 and 13). Surprisingly, however, increased abundances of both species correlate with nonsapropel intervals at greater depths, particularly in the hemipelagic muds between sapropels S3, S4, and S5, which accumulated during MIS 5 (Figures 4–8). This difference in the behaviour of *G. bulloides* and *G. ruber* (white) between S1 and older sapropels S3, S4, and S5 indicates a significant difference in nutrient levels and structure of the water column from MIS 5 to MIS 1. Because *G. bulloides* and *G. ruber* are known to inhabit eutrophic and oligotrophic waters, respectively, their cooccurrence is potentially problematic and is discussed further, below (under Ecozone IV).

### 4.2. Significance of downcore distribution of N. pachyderma (d)

*N. pachyderma* (d) is either absent or has very low percentages in sapropel S1, whereas the older sapropels

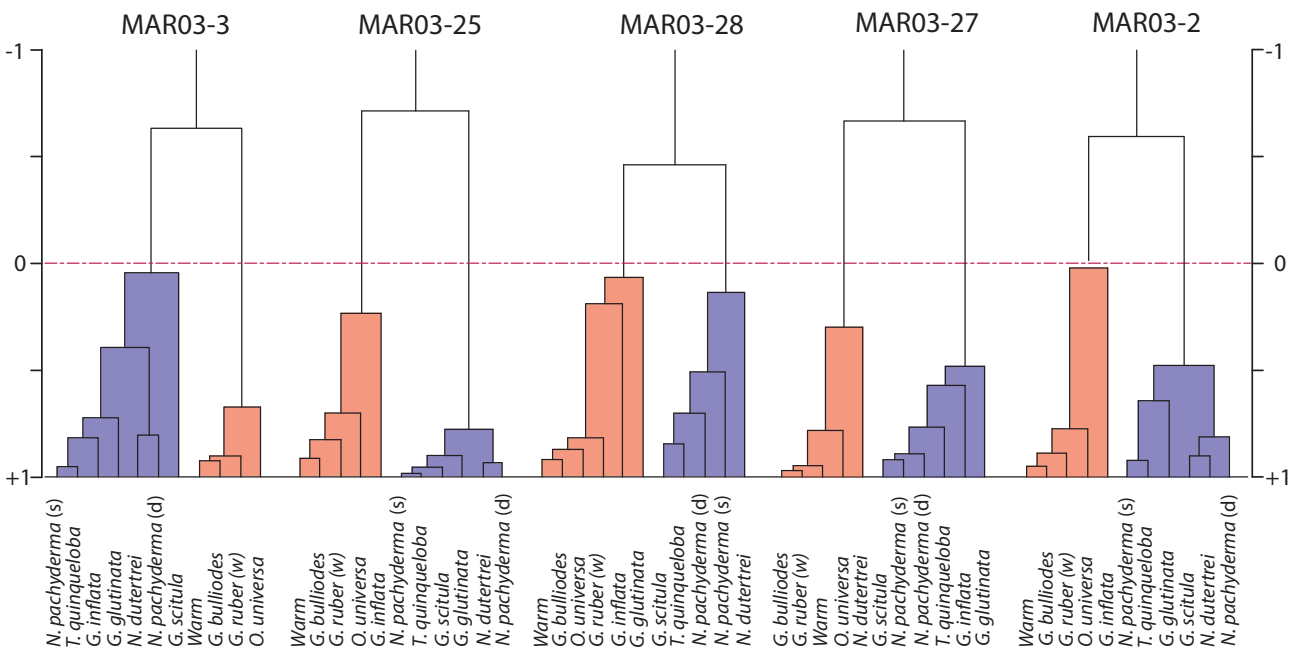


**Figure 13.** Dendrograms resulting from R-mode hierarchical cluster analysis (centroid linkage method, distance metric is 1-Pearson correlation coefficient); warm = sum of tropical species.

S3, S4, and S5 contain 50%–70% *N. pachyderma* (d). This situation is also observed in other eastern Mediterranean cores (e.g., Thunell et al., 1977; Rohling and Gieskes, 1989; Rohling et al., 1993). *N. pachyderma* (d) is rare to absent in oligotrophic waters, but its presence is well documented in eutrophic waters closely associated with development of a deep chlorophyll maximum. A deep chlorophyll maximum develops when the pycnocline lies close to the base of, or within, the euphotic zone where there is enough light for primary production (Rohling and Gieskes, 1989; Rohling et al., 1993). Rising of the pycnocline occurs when the density contrast between the intermediate and surface water decreases and, under such conditions, the nutricline usually is found closely associated with the pycnocline.

In the modern Aegean Sea, the surface water layer consists mainly of brackish Black Sea outflow, whereas intermediate water is more saline Mediterranean Intermediate Water. Hence, the pycnocline depth (essentially a halocline) is regulated mainly by the rate of freshwater/brackish water input, modulated by evaporation and winter cooling. In this context, the downcore frequency distribution of *N. pachyderma* (d) can be interpreted as a record of the interactions between surface and intermediate waters of the Aegean Sea, and perhaps temporal changes in the end-member properties of these water masses.

### 4.3. Significance of downcore distribution of stable carbon isotopes ($\delta^{13}C$)

Inorganic carbon isotope signals reflect changes that occurred within the surface water layer and, to a lesser extent, the upper portions of the intermediate water mass. This is where planktonic foraminifera dwell during their life span. Theoretically, surface and deep waters should display, respectively, heavier (most $^{13}C$ enriched) and lighter $\delta^{13}C_{DIC}$ values in the water column, because $^{12}C$ is preferentially sequestered by marine algae during photosynthesis within the euphotic layer and subsequently transferred from the surface layers to deeper water by postmortem settling of organic material (referred to as the biological pump, Rohling et al., 2004). Foraminifera living in such surface waters would form calcite tests enriched in $^{13}C$. However, in areas where enhanced river input occurs, surface waters can exhibit depleted $\delta^{13}C$ values due to the light carbon content of the freshwater that can range from –5‰ to –10‰ (inorganic carbon) to as light as –27‰ (suspended organic carbon; Fontugne and Calvert, 1992). For example, the $\delta^{13}C$ composition of the surface water in the Black Sea is approximately –13‰ (Abrajano et al., 2002). In semienclosed marine settings with significant river inputs, the effect of biological pumping is masked by light carbon dilution, and foraminifera are expected to have depleted $\delta^{13}C$ values.

In the studied cores, stable carbon isotopes in planktonic foraminifera show maximum depletions during and/or immediately below sapropels (Figure 10). If biological pumping was the dominant control on surface-water isotopic composition, then depleted planktonic foraminiferal $\delta^{13}C$ values might reasonably indicate low primary productivity in the surface waters. However, the Aegean Sea is surrounded by numerous freshwater/brackish water sources, and so the light carbon isotopic values in the foraminiferal tests cannot be used to assess changes in primary productivity, and more likely record changes in freshwater/brackish water supply. Uninterrupted presence of benthic foraminifera in all samples, including sapropels, strongly suggests that bottom waters were not anoxic, but reached dysoxic levels. During the deposition of the MIS 5 sapropels S3, S4, and S5, the notable depletion in benthic foraminiferal $\delta^{13}C$ values can be explained by minor amounts of vertical mixing with depleted $\delta^{13}C_{DIC}$ from the surface waters, leading to a degree of ventilation (oxygenation) that prevented bottom-water anoxia.

### 4.4. Ecozones

Stratigraphic trends in the distribution of the most common taxa (*N. pachyderma* (d), *G. bulloides*, *G. ruber*, *G. inflata*) are very similar in all five cores studied from the Aegean Sea, suggesting that major changes in surface-water characteristics took place more or less synchronously throughout the Aegean Sea since ~130 ka.

**Ecozone IV (>60 ka)**

Ecozone IV spans a time interval during which successive moderate amplitude fluctuations are observed in SST, SSS, and $\delta^{13}C$ values, and in the frequency distributions of the most common taxa (i.e. *N. pachyderma* (d), *G. ruber*, and *G. bulloides*). Sapropels S3, S4, and S5 accumulated under these conditions (Figures 4–11). A close covariation of *G. ruber* and *G. bulloides* is consistently observed during deposition of nonsapropel sediments within Ecozone IV (Figure 14a). *G. ruber* is a warm oligotrophic mixed-layer dweller, whereas *G. bulloides* is highly dependent on enhanced food levels with no depth preference. The covariation is consistent with stratification of the euphotic zone, with a warmer and nutrient-poor upper layer and a cooler lower layer with high nutrient content. Such conditions could provide favorable habitats for both species to thrive at slightly different depths in the water column. The dominance of *N. pachyderma* (d) during times of sapropel formation indicates the establishment of a sustained and distinct deep chlorophyll maximum layer within the euphotic zone (Figures 14b and 14c). Such conditions require stratification of the water column and shoaling of the pycnocline into the euphotic ecozone. The formation of a deep chlorophyll maximum layer is promoted by increased river runoff, which is consistent with decreased sea surface temperatures and the observed depletions in $\delta^{13}C$ values. Another important observation is the close association of *N. dutertrei* with

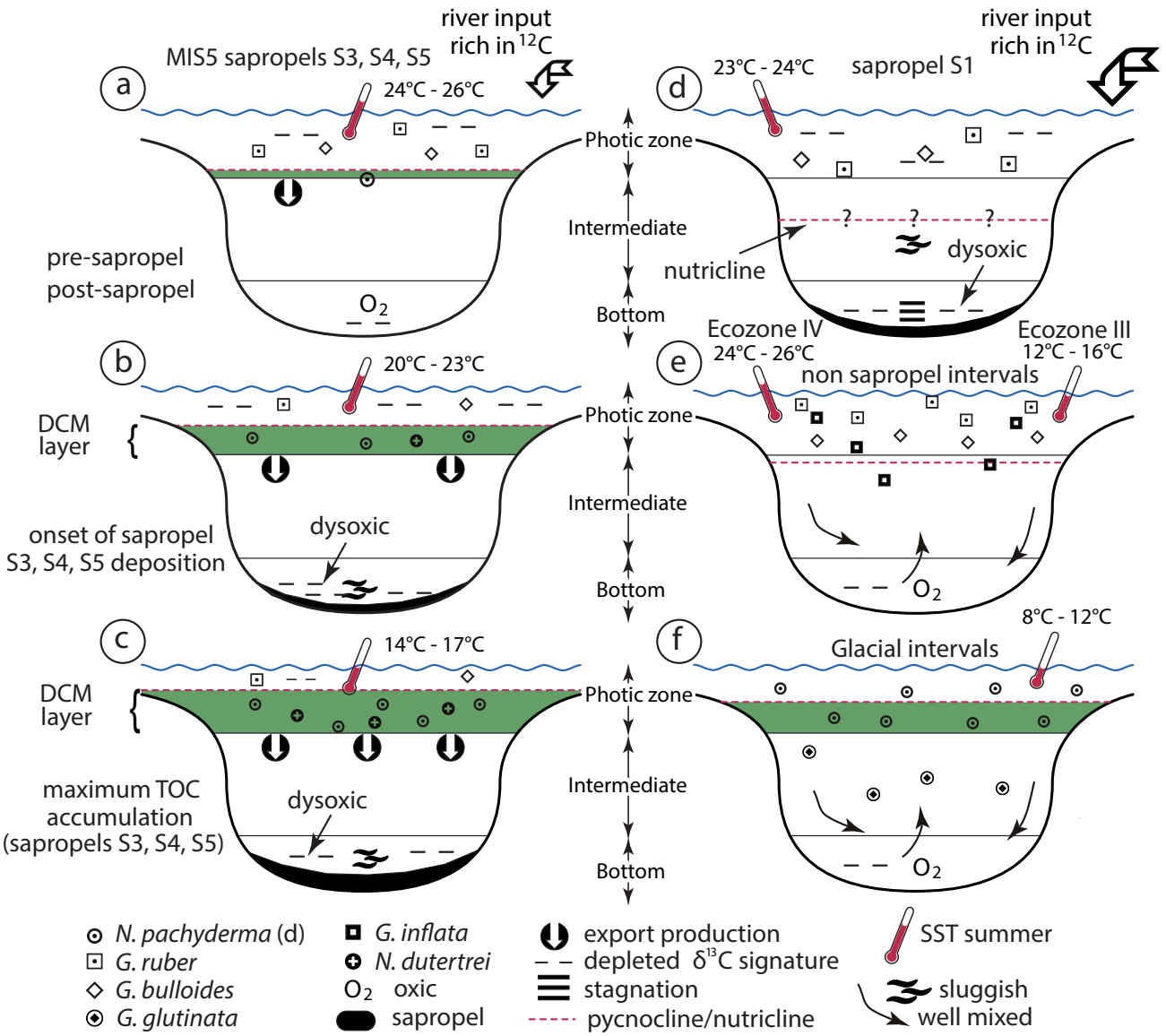


**Figure 14.** Schematic demonstration of water column hydrographic conditions during the formation of sapropels S3, S4, and S5 (part a = presapropel and postsapropel, part b = sapropel onset, part c = height of sapropel development); sapropel S1 (part d); nonsapropel layers (part e), and glacial times (part f). Green tone marks deep chlorophyll maximum.

sapropels S3, S4, and S5 and the peak abundances of *N. pachyderma* (d). The subsurface-dwelling foraminifera *N. dutertrei* is exclusively herbivorous and so its population increases after phytoplankton blooms (Thunell and Reynolds, 1984; Hemleben et al., 1989). The appearance of *N. dutertrei* during times of maximum abundances of *N. pachyderma* (d) might record the shallowest position of the deep chlorophyll maximum layer, well into the euphotic zone, when large phytoplankton populations would be expected (Figure 14c). In addition, the highest organic carbon concentrations also coincide with the presence of *N. dutertrei*, suggesting a positive correlation between shoaling of the deep chlorophyll maximum and enhanced organic carbon deposition. The presence of *G. inflata* in sapropel S4 in all cores studied is a notable difference in the MIS5 sapropels (Figures 4 and 6–8). The persistent and relatively high abundances of *G. inflata* in the cores from the Aegean Sea strongly suggest enhanced vertical mixing, at least during the winters (i.e. Pujol and Vergnaud-Grazzini, 1995).

The development of a deep chlorophyll maximum layer during the deposition of sapropels S3, S4, and S5 has been suggested for the southernmost Aegean Sea by other researchers (Rohling and Gieskes, 1989). Core

T87/2/27 is a 3-m-long gravity core that was collected immediately southwest of the Island of Antikythera (Figure 1; Rohling and Gieskes, 1989). Four sapropel/sapropelic mud layers were identified in this core and were tentatively correlated with the oxygen isotopic record of RC-9 181, a core recovered from the Mediterranean Ridge south of Crete (33°25′N & 25°00′E – 2286 m water depth; Vergnaud-Grazzini et al., 1977). Rohling and Gieskes (1989) correlated these sapropels with S1, S3, S4, and S5 and suggested that the absence of neogloboquadrinids in S1 and their abundance in S3, S4, and S5 reflect differences in food availability related to the extent of development of a deep chlorophyll maximum layer and the intensity of primary production associated with this layer. They argued that the depth of the deep chlorophyll maximum layer is determined by the vertical structure of the water column, and suggested that the pycnocline was positioned well above the base of the euphotic zone during deposition of sapropels S3, S4, and S5. Core LC21 is a 13.5-m-long piston core collected from the eastern Cretan Trough, west of the islands of Kasos and Karpathos (Figure 1; Rohling et al., 2004; Marino et al., 2009; Osbourne et al., 2010). This core has been the focus of extensive paleoceanographic research and has become the best understood sapropel record in the eastern Mediterranean Sea (Rohling et al., 2004; Marino et al., 2009; Osbourne et al., 2010). Sapropels S1 and S3–S5 were identified in LC21, although previous studies have generally focused on sapropels S1 and S5, with no major work on sapropels S3 and S4. The chronostratigraphy of the core was established through radiocarbon dating in the upper part of the core and by correlation to the Soreq Cave speleothem data (Bar-Matthews et al., 2003; 2009) for the age of S5. Previous studies showed that sapropel S5 accumulated under conditions of enhanced freshwater dilution of surface waters, elevated productivity, shoaling of the pycnocline between intermediate and surface waters, and stagnation of the subsurface circulation (Rohling et al., 2004). Freshwater contributions to the Aegean Sea during the deposition of sapropel S5 were traced using Nd isotopes in planktonic foraminifera (Osbourne et al., 2010), possible because radiogenic sources are most widespread to the south, in Africa, whereas nonradiogenic sources are found to the north. These data showed that the most likely source for freshwater was rivers flowing northward from the central Saharan watershed. Osbourne et al. (2010) concluded that there was no large influx of water from the north during the deposition of sapropel S5.

During the formation of MIS 5 sapropels S3, S4, and S5, $\delta^{18}O$ and sea surface temperature/salinity values show contradictory relationships: depletions in oxygen isotope values coincide with decreased SST and SSS values. Although not commonly observed, drops in sea surface temperatures of 2 °C (S5) and 6 °C (S4) have also been observed from the eastern Mediterranean Sea in core MD84-641 collected off the Nile River where increasing surface temperatures are associated with $\delta^{18}O$ enrichments in the planktonic foraminifera *G. ruber* (Kallel et al., 2000). The association of lower SST/SSS values with more negative $\delta^{18}O$ values in the cores can be attributed to the presence of less saline cool waters and/or increased precipitation.

In this study, benthic foraminiferal assemblages are not described in detail; however, benthic foraminifera were examined in samples from sapropels S3, S4, and S5. These samples contained a low-abundance and low-diversity benthic foraminiferal fauna dominated by *Globobulimina affinis*, *G. pseudospinescens*, *Chilostomella mediterranensis*, *Bolovina alata*, *B. attica*, *Bulimina clara*, and *Uvigerina peregrina curticosta*. This benthic foraminiferal faunal assemblage indicates nutrient-rich, oxygen-poor bottom waters during the deposition of MIS 5 sapropels S3, S4, and S5. *G. affinis*, *G. pseudospinescens*, and *C. mediterranensis* co-occurring with *Bolivina* species are also reported in several sapropels from the eastern Mediterranean Sea (Cita and Podenzani, 1980; Herman, 1981; Mullineaux and Lohmann, 1981; Stefanelli et al., 2005; Abu-Zied et al., 2008; Melki et al., 2010) and are known to be abundant in oxygen-poor (dysoxic) bottom water conditions (Ross and Kennett, 1984; McCorkle et al., 1990; Stefanelli et al., 2005; Abu-Zied et al., 2008; Melki et al., 2010).

The depleted planktonic and benthic $\delta^{13}C$ values are interpreted to be a consequence of river runoff bringing $^{12}C$-enriched nutrients, and a distinct deep chlorophyll maximum layer situated well within the euphotic layer providing additional nutrients that resulted in augmented $^{12}C$-enriched 'export' to the sea floor (Figure 14c). Furthermore, close covariation between benthic and planktonic $\delta^{13}C$ signals suggests that deep waters inherited their carbon from surface waters via the export of organic detritus from the upper part of the water column and limited vertical mixing. Coincident depletions/enrichments both in carbon and oxygen isotope values support the hypothesis that fluvial $^{12}C$- and $^{16}O$-enriched waters controlled the isotopic composition in the semienclosed Aegean Sea.

Pollen records, both terrestrial (i.e. Ionnina - western Greece, Tenaghi Philippon - northeastern Greece; Mommersteeg et al., 1995; Tzedakis et al., 1997, 2006) and marine (MD84-627 and MD84-642 - northeast off the Nile River), show that climatic conditions during interstadials were humid and warm, characterized by high abundances (to 97%) of arboreal pollen (e.g., *Quercus*, *Pinus*, *Pistacia* Figure 15), whereas stadials were cooler and more arid (e.g., increase in *Artemisia*; Tzedakis et al., 1997; Cheddadi and Rossignol-Strick, 1995; Mommersteeg et al., 1995). Maximum depletions in the foraminiferal $\delta^{13}C$ and $\delta^{18}O$ signals in the Aegean Sea cores are in good agreement

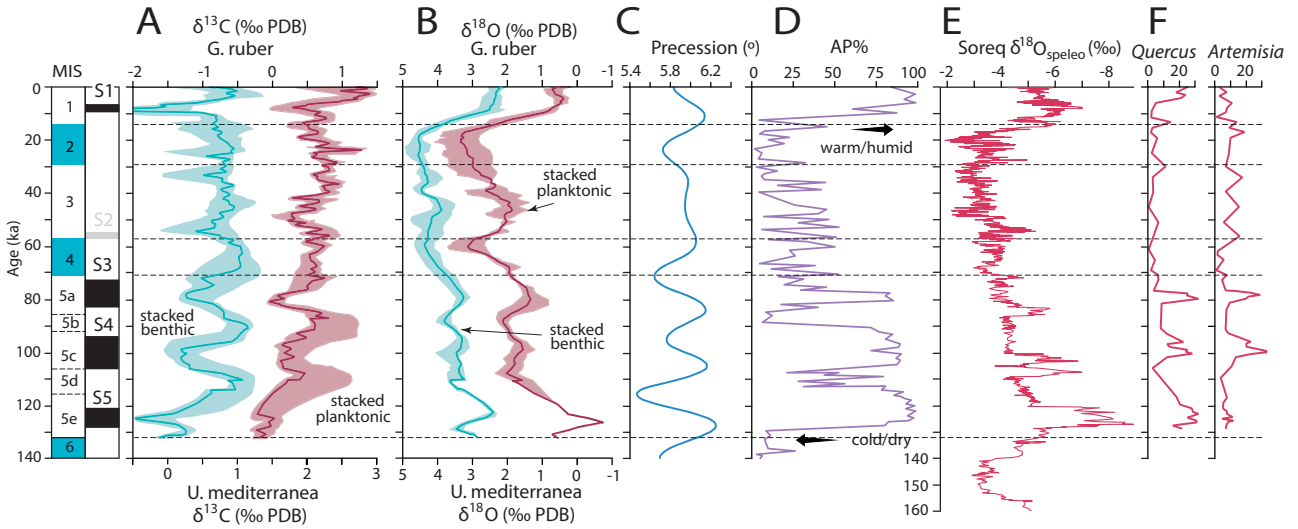


**Figure 15.** Comparison of stacked $\delta^{13}C$ and $\delta^{18}O$ curves from this study with pollen records from NE Greece and the eastern Mediterranean. (A) stacked $\delta^{13}C$ curves in planktonic and benthic foraminifera; (B) stacked $\delta^{18}O$ curves in planktonic and benthic foraminifera; (C) precession curve; (D) arboreal pollen (AP) percentage curve from Tenaghi Philippon sequence, NE Greece (modified from Tzedakis et al., 2003); (E) Soreq Cave $\delta^{18}O_{speleo}$ record (modified from Grant et al., 2012); (F) downcore variations of Quercus and Artemisia species (wet/warm-forest and arid/cool climate indicators, respectively) in MD84-627 (off the Nile River; modified from Cheddadi and Rossignol-Strick, 1995).

with increased arboreal pollen percentages particularly during interstadial stage 5a. However, rather 'short lived' isotopic depletions during the deposition of sapropels S5 and S4 do not reflect the extended periods of high arboreal pollen encompassing the entire interstadial stages 5e and 5c. Instead, the depletions coincide well with times of maximum insolation (with ~3 kyr lag) suggesting that the intensity of the monsoon system played an important role in the climatic conditions over the Aegean Sea (Figure 15). There is also a remarkable correlation between the ~150 kyr $\delta^{18}O$ and $\delta^{13}C$ record determined from speleothems of the Peqiin Cave in Israel and the stable isotopic records from the Aegean Sea cores (Figure 15; Bar-Matthews et al., 2003; Grant et al., 2012). This correlation provides a strong linkage between the regional terrestrial climatic signal, reflecting the variations in land temperature and rainfall, and the oceanic climate reflected in SSTs, SSTw, and SSSw records. The correspondence of low $\delta^{18}O$ speleothem values with low *G. ruber* $\delta^{18}O$ values in the Aegean Sea cores during interglacial sapropel events S3, S4, and S5 indicates that these periods were characterized by enhanced rainfall in the eastern Mediterranean region, over both land and sea (Figure 15; Bar-Matthews et al., 2003; Grant et al., 2012).

In the eastern Mediterranean Sea, the MIS 5 sapropels were deposited during substages 5a (sapropel S3), 5c (sapropel S4), and 5e (sapropel S5) and are in some instances associated with $\delta^{18}O$ depletions and increased sea surface temperatures (e.g., Mulitza et al., 2003) and in other instances with decreased sea surface temperatures (e.g., Kallel et al., 2000). Similarly, depleted oxygen isotope values are observed in MIS 5 sapropels from the Aegean Sea (Figures 9, 11, and 12). However, the planktonic foraminiferal $\delta^{18}O$ values are more enriched than in their counterparts from the eastern Mediterranean Sea, corresponding to ~5 °C lower sea surface temperatures (Figures 11 and 12), and are more similar to core MD84-641 off the Nile River (Kallel et al., 2000). This enrichment is probably caused by temperature differences rather than by higher salinity considering the confined geographic position of the Aegean Sea and the high fresh/brackish water input by the surrounding rivers and Black Sea outflow. If true, these enriched $\delta^{18}O$ signals support the presence of cooler surface waters during the formation of MIS 5 sapropels in the Aegean Sea with respect to those in the eastern Mediterranean Sea.

**Ecozone III (60–40 ka)**

The reappearance of *G. inflata* and decreased percentages of *N. pachyderma* (d) in ecozone III indicate a weaker stratification of the surface waters than was the case for subecozone IVa (Figure 14d). In the southern cores MAR03-25 and MAR03-02, higher abundances of *G. inflata* reaching 36% and low abundances of *N. pachyderma* (d) together suggest the presence of a stronger vertical mixing of the surface waters than at other core localities. These hydrographic conditions show similarities to those that existed during nonsapropel times in Ecozone IV (see above); however, the SST values for Ecozone III

are significantly lower by as much as 4 °C, consistent with relatively enriched $\delta^{18}O$ signatures and lower *G. ruber* abundances.

Higher percentages of *N. pachyderma* (d) and *T. quinqueloba* at the upper and lower boundaries of Ecozone III suggest cooler and less saline surface waters, confirmed by SST and SSS plots (Figure 11). *G. glutinata* appears for the first time within the upper portions of Ecozone III, signaling the initial stages of glacial conditions associated with the transition into MIS 2. Furthermore, the SST plots show that the temperature drop of 2–4 °C toward the top of the ecozone is more pronounced than the earlier drop at the lower boundary (Figure 11).

**Ecozone II (40–12.5 ka)**

During the development of Ecozone II, the upward increase in the abundance of *N. pachyderma* (d) together with the presence of *N. pachyderma* (s) and *T. quinqueloba* indicate progressive cooling into a cold interval corresponding to the glacial MIS 2 (Figure 14e). This climatic change is also demonstrated by enrichment in $\delta^{18}O$ values and decreased surface water temperatures. The planktonic foraminiferal SST and Mg/Ca SST calculations show that water temperatures ranged between 11 °C and 15 °C, about 6 °C cooler than today (Figure 12). Ecozone II demonstrates similar frequency distributions (e.g., dominance of *N. pachyderma* (d), decreased *G. ruber* and *G. bulloides* percentages) to those observed in subecozones IV a, c, and e, suggesting that similar water masses existed during glacial periods and during times of formation of sapropels S3, S4, and S5 (Figures 11, 14e versus 14b).

An important difference in Ecozone II is that sedimentation took place under oxygenated bottom water conditions unfavorable for increased organic carbon preservation (Figure 14e). The dominance of *N. pachyderma* (d) during MIS 2 places constraints on the conditions prevailing during the deposition of MIS 5 sapropels. During MIS 2 as well as the sapropel intervals of MIS 5 there was a permanent pycnocline within the euphotic zone, and the density contrast between intermediate and surface waters was of similar magnitude. The proposed shallow position of the permanent pycnocline during MIS 2 can be explained by glacioeustatic sealevel lowering, as has been hypothesized for the eastern Mediterranean Sea (Rohling and Gieskes, 1989; Rohling, 1991). There, a shallow permanent pycnocline and related frequency increases in neogloboquadrinids during glacial periods are attributed to glacioeustatic sealevel lowering that resulted in a reduction in inflow across the Strait of Sicily (Rohling, 1991). Similar conditions could easily be envisaged for the semienclosed Aegean Sea where reduced inflow from the eastern Mediterranean Sea and the Black Sea could cause comparable conditions with less buoyancy contrast between the surface and the intermediate waters, resulting in a shallower pycnocline. Episodic appearances of *G. inflata*, an indicator of a cool and homogeneous winter mixed layer, during the formation of MIS 5 sapropels and its complete absence throughout Ecozone II are suggestive of a sustained/stronger stratification of the water column particularly during glacial times (e.g., MIS 2). However, the fact that bottom water oxygen deficiency did not develop throughout the entire glacial time span implies that surface water temperatures were sufficiently low to promote downwelling, permitting bottom water replenishment, and accordingly precluding sapropel formation.

**Ecozone I (12.5 ka–present)**

The dominance of *G. ruber* in Ecozone I together with relatively high abundances of warm water species indicates the establishment of fully interglacial conditions (Figure 14f). The SST calculations support the presence of warm waters that mainly ranged between 17 °C and 24 °C (Figures 11 and 12). Rohling and Gieskes (1989) also suggested that during the deposition of sapropel S1 the pycnocline vanished due to termination of Mediterranean Intermediate Water formation and that there was no deep chlorophyll maximum. Significant depletions in $\delta^{13}C$ values, particularly during sapropel S1 accumulation, suggest excessive amounts of freshwater and/or brackish water input to the Aegean Sea, most likely from the Black Sea and rivers draining into the Black Sea and possibly in lesser amounts from the Nile River (Figure 10). Other workers also have suggested that fresh/brackish water outflow from the Black Sea during the MIS 2/1 transition is mainly responsible for the development of sapropel S1 (Aksu et al., 1995; Hiscott et al., 2007a, 2007b).

The above interpretation requires that the Black Sea was connected to the Aegean Sea through the Marmara Sea at, or immediately before, the onset of deposition of the most recent sapropel S1. The late MIS 2 and Holocene reconnection of the Black Sea to the world ocean is hotly debated in the literature. Hiscott et al. (2007a, 2007b) have provided arguments supporting persistent Black Sea outflow to the world ocean starting at ~11.7 cal ka, including the period of M1 and S1 sapropel deposition in the Marmara and Aegean seas, ~11.9–6.75 cal ka (Çağatay et al., 2000) and ~9.9–6.6 cal ka respectively. Thom (2010) modeled the hydrological budget of the Black Sea through the late Quaternary and concluded that the Black Sea must have been exporting water to the world ocean during S1 time. Other workers have disagreed based on isotopically based estimates of SST and SSS using alkenone biomarkers and oxygen isotopic variations (Sperling et al., 2003; Vidal et al., 2010), noting higher SSS values during M1/S1 time that are apparently inconsistent with Black Sea outflow. Vidal et al. (2010) suggested that the Marmara Sea only became reconnected to the Black Sea between 9 and 8 cal

ka, ~1000 years after the onset of sapropel deposition in the Aegean Sea. Çağatay et al. (2009) have provided an explanation for sapropel M1 in the Marmara Sea that has no genetic link with conditions that led to the deposition of essentially coeval S1 in the Mediterranean Sea and no link with Black Sea outflow. They proposed that intrusion of saline Mediterranean water, starting at ~13.4 cal ka (calibrated from ~12 $^{14}$C ka) forced the ambient fresher waters to the surface and eventually out through the Dardanelles Strait, creating water-column stratification and bottom-water dysoxia in the Marmara Sea that, with a significant time lag, promoted sapropel formation.

The assessments by Sperling et al. (2003) and Vidal et al. (2010) of a higher, rather than lower, SSS in the Marmara Sea during S1 deposition in the Aegean Sea might not actually rule out Black Sea outflow at that time. This is because the isotopic data underpinning the SSS estimates come from the remains of marine algae and foraminifera that do not tolerate the low salinity of surface waters in the Marmara Sea, even today when those surface waters have a salinity of ~20 psu down to a depth of ~25 m (Aksu et al., 2002). Vidal et al. (2010) proposed that these organisms lived in the region of the contemporary pycnocline, but if the SSS estimates recently published by Mertens et al. (2012) and Bradley et al. (2012) are correct, then any early Holocene Black Sea outflow would have had a significantly lower salinity of ~7–14 psu, effectively toxic to the marine organisms used by Sperling et al. (2003) and Vidal et al. (2010) for their SSS estimates. Hence, their alkenone and oxygen-isotopic data must record the water temperature and salinity within the top of the saline deeper water mass of the Marmara Sea, above which a low-salinity sheet of Black Sea outflow might have been flowing, undetected by their methods, toward the Aegean Sea. Until there is stronger, unambiguous evidence that Black Sea outflow could not have been possible during S1 time, the interpretation presented in this paper to explain the creation of a low-salinity lid preventing bottom-water ventilation in the Aegean Sea remains viable. Furthermore, the genesis of largely contemporaneous sapropels M1 and S1 can be explained in a consistent manner if Black Sea outflow was a trigger, rather than needing fully independent mechanisms for similar and synchronous organic-rich deposits in such close geographic proximity.

The notable drop in $\delta^{13}$C values during the deposition of sapropel S1 coincides with only minor cooling of surface water temperatures (Figure 11). The lack of greater cooling at this time can be ascribed to the warmer temperatures of the Black Sea outflow into the Aegean Sea, as surface waters likely warmed while flowing across the Marmara Sea on their way to the Aegean Sea (Poulos et al., 1997; Zervakis and Georgopoulos, 2002). The abrupt disappearance of *N. pachyderma* (d) during deposition of S1 suggests unfavorable conditions for the development of a deep chlorophyll maximum layer. This might have been caused by deepening of the pycnocline far below the euphotic ecozone (Figure 14f) or even by complete disruption of the pycnocline. This situation would require a near-complete shutdown of intermediate water formation, causing a diminished oxygen supply at intermediate depths, thus resulting in strongly stagnant bottom water conditions (e.g., Rohling and Gieskes, 1989). Increased abundances of *G. bulloides* during deposition of S1 have also been recognized in the Adriatic Sea (Jorissen et al., 1993; Rohling et al., 1993) and by other workers in the Aegean Sea (e.g., Geraga et al., 2010) and have been attributed by those authors to increased river discharges creating high nutrient levels.

Stratification occurs in the water column when there is a high density contrast between the surface mixed layer and the intermediate and/or bottom waters. Stagnation can take place locally in bottom waters where there is strong vertical stratification. A stratified water column would diminish or even halt the vertical advection of oxygenated surface waters resulting in sluggish/stagnant bottom waters. In shallow basins with a thin surface layer, stratification can be broken during intense storms, which would cause the thermocline/nutricline to rise well within the surface mixed layer. As a result, nutrient-rich waters would increase the rate of photosynthesis, enhancing primary production. Stagnation can also occur in regions where there is a marked reduction (or cessation) in the rate of bottom water formation.

Quantitative variations in the planktonic faunal assemblages identified in five cores collected from the northern to southern Aegean Sea support the following conclusions. Sapropels S3, S4, and S5 were deposited under similar hydrographic conditions with a distinct deep chlorophyll maximum layer, a stratified water column, and increased primary productivity. Sapropel S1 was deposited in the absence of a deep chlorophyll maximum layer, so that the water column lacked a deep phytoplankton assemblage. Under such conditions, oxygen advection via intermediate water flow must have been significantly reduced, which implies significant stagnation. Leading up to the deposition of sapropels S3, S4, and S5, modifications in the hydrographic conditions were initiated ~5–7 kyr before the onset of sapropel deposition. The sapropels predominantly coincided with maximum depletions in $\delta^{13}$C and lowest SST values. The dominant factor for the formation of MIS 5 sapropels was an increase in primary productivity; however, the presence of sluggish intermediate water with weakened bottom water replenishment cannot be discounted. The formation of sapropel S1 is attributed to intense fresh/brackish water input, which resulted in strong stratification and the near stagnation of the bottom water.

Cluster analysis shows consistent coupling of *G. bulloides* with *G. ruber* during times of nonsapropel deposition, which is interpreted to suggest a stratified euphotic zone composed of a warm/nutrient-poor and a cooler/nutrient-rich upper and lower layer, respectively. This covariation further points to increased river runoff to explain the fertility and stratification of the surface waters. In sapropel layers S3, S4, and S5, appearances of *N. dutertrei* are interpreted to represent maximum shoaling of the pycnocline and highest levels of primary productivity.

**Acknowledgements**
We thank Dr Doğan Yaşar for his continued support and the officers and crew of the *RV Koca Piri Reis* of the Institute of Marine Sciences and Technology, Dokuz Eylül University, for their assistance in data acquisition. We acknowledge research and ship-time funds from the Natural Sciences and Engineering Research Council of Canada (NSERC) to Aksu and Hiscott, travel funds from the Dean of Science, Memorial University of Newfoundland, and a special grant from the Vice President (Research), Memorial University of Newfoundland. We thank Alison Pye for her assistance in the stable isotopic and elemental analyses.

## References

Abrajano T, Aksu AE, Hiscott RN, Mudie PJ (2002). Aspect of carbon isotope biogeochemistry of Late Quaternary sediments from the Marmara Sea and Black Sea. Mar Geol 190: 151–164.

Abu-Zied RH, Rohling EJ, Jorissen FJ, Fontanier C, Casford JSL, Cooke S (2008). Benthic foraminiferal response to changes in bottom-water oxygenation and organic carbon flux in the eastern Mediterranean during LGM to Recent times. Mar Micropaleontol 67: 46–68.

Aksu AE, Yaşar D, Mudie PJ (1995a). Paleoclimatic and paleoceanographic conditions leading to development of sapropel layer S1 in the Aegean Sea basins. Palaeogeogr Palaeoecol 116: 71–101.

Aksu AE, Yaşar D, Mudie PJ, Gillespie H (1995b). Late glacial - Holocene paleoclimatic and paleoceanographic evolution of the Aegean Sea: micropaleontological and stable isotopic evidence. Mar Micropaleontol 25: 1–28.

Aksu AE, Hiscott RN, Mudie PJ, Rochon A, Kaminski M, Abrajano T, Yaşar D (2002). Persistent Holocene outflow from the Black Sea to the eastern Mediterranean contradicts Noah's Flood hypothesis. GSA Today 12: 4–10.

Aksu AE, Jenner G, Hiscott RN, İşler EB (2008). Occurrence, stratigraphy and geochemistry of Late Quaternary tephra layers in the Aegean Sea and the Marmara Sea. Mar Geol 252: 174–192.

Anand P, Elderfield H, Conte MH (2003). Calibration of Mg/Ca thermometry in planktonic foraminifera from a sediment trap time series, Paleoceanography 18: 1050, doi:10.1029/2002PA000846.

Bar-Matthews M, Ayalon A, Gilmour M, Matthews A, Hawkesworth CJ (2003). Sea–land oxygen isotopic relationships from planktonic foraminifera and speleothems in the Eastern Mediterranean region and their implication for paleo-rainfall during interglacial intervals. Geochim Cosmochim Ac 67: 3181–3199.

Bé AWH, Spero HJ, Anderson OR (1982). Effect of symbiont elimination and reinfection on the life processes of the planktonic foraminifera *Globigerinoides sacculifer*: Mar Biol 70: 73–86.

Berger A (1978). Long-term variations of daily insolation and Quaternary climate changes. J Atmos Sci 35: 2362–2367.

Berger A, Mélice JL, Loutre MF (2005). On the origin of the 100-kyr cycles in the astronomical forcing. Paleoceanography, 20: PA4019, doi:10.1029/2005PA001173.

Berger A, Loutre MF, Mélice JL (2006). Equatorial insolation: from precession harmonics to eccentricity frequencies. Clim Past 2: 131–136.

Bradley LR, Marret F, Mudie PJ, Aksu AE, Hiscott RN (2012). Constraining Holocene sea-surface conditions in the southwestern Black Sea using dinoflagellate cysts. J Quaternary Sci 27: 835–843.

Çağatay MN, Görür N, Algan A, Eastoe CJ, Tchapalyga A, Ongan D, Kuhn T, Kuscu I (2000). Late Glacial – Holocene palaeoceanography of the Sea of Marmara timing of connections with the Mediterranean and the Black Sea. Mar Geol 167: 191–206.

Çağatay MN, Eriş K, Ryan WBF, Sancar U, Polonia A, Akçer S, Biltekin D, Gasperini L, Görür N, Lericolais G et al. (2009). Late Pleistocene-Holocene evolution of the northern shelf of the Sea of Marmara. Mar Geol 265: 87–100.

Casford JSL, Rohling EJ, Abu Zied RH, Cooke S, Fontanier C, Leng M, Lykousis V (2002). Circulation changes and nutrient concentrations in the late Quaternary Aegean Sea: a non-steady state concept for sapropel formation. Paleoceanography 17: 1024, DOI:10.1029/2000PA000601.

Cheddadi R, Rossignol-Strick M (1995). Improved preservation of organic matter and pollen in Eastern Mediterranean sapropels. Paleoceanography 10: 301–309.

Cita MB, Podenzani M (1980). Destructive effects of oxygen starvation and ash falls on benthic life: a pilot study. Quaternary Res 13: 230–241.

Dekens PS, Lea DW, Pak DK, Spero HJ (2002). Core top calibration of Mg/Ca in tropical foraminifera: refining paleotemperature estimation. Geochem Geophys Geosys 3: 1022, doi:10.1029/2001GC000200.

Edgar KM, Bohaty SM, Gibbs SJ, Sexton PF, Norris RD, Wilson PA (2013). Symbiont 'bleaching' in planktic foraminifera during the Middle Eocene Climatic Optimum. Geology 41: 15–18.

Emeis KC, Schulz H, Struck U, Rossignol-Strick M, Erlenkeuser H, Howell MW, Kroon D, Mackensen A, Ishizukam S, Oba T et al. (2003). Eastern Mediterranean surface water temperatures and $\delta^{18}O$ composition during deposition of sapropels in the late Quaternary. Paleoceanography 18: 1005. doi:10.1029/2000PA00061.

Emeis KC, Sakamoto T, Wehausen R, Brumsack HJ (2000). The sapropel record of the eastern Mediterranean Sea—results of Ocean Drilling Program Leg 160. Palaeogeogr Palaeoecol 158: 371–395.

Facorellis Y, Maniatis Y, Kromer B (1998). Apparent 14C ages of marine mollusk shells from a Greek island: calculation of the marine reservoir effect in the Aegean Sea. Radiocarbon 40: 963–973.

Ferguson JE, Henderson GM, Kucera M, Rickaby REM (2008). Systematic change of foraminiferal Mg/Ca ratios across a strong salinity gradient. Earth Planet Sc Lett 265: 153–166.

Fontugne MR, Calvert SE (1992). Late Pleistocene variability of the carbon isotopic composition of organic matter in the eastern Mediterranean: monitor of changes in carbon sources and atmospheric CO2 concentrations. Paleoceanography 7: 1–20.

Geraga M, Tsaila Monopolis St, Ioakim Ch, Papatheodorou G, Ferentinos G (2005). Short term climate changes in the southern Aegean Sea over the last 48,000 years. Palaeogeogr Palaeoecol 220: 311–332.

Geraga M, Ioakim Chr, Lykousis V, Tsalia-Monopolis St, Mylona G (2010). The high-resolution palaeoclimatic and palaeoceanographic history of the last 24,000 years in the central Aegean Sea, Greece. Palaeogeogr Palaeoecol 287: 101–115.

Grant KM, Rohling EJ, Bar-Matthews M, Ayalon A, Medina-Elizalde M, Bronk Ramsey C, Satow C, Roberts AP (2012). Rapid coupling between ice volume and polar temperature over the past 150,000 years. Nature 491: 744–747.

Grimm EC (1987). CONISS: a FORTRAN 77 program for stratigraphically constrained cluster analysis by the method of incremental sum of squares. Comput Geosc 13: 13–35.

Hemleben C, Spindler M, Anderson OR (1989). Modern Planktonic Foraminifera. Heidelberg, Germany: Springer Verlag.

Herman Y (1981). Paleoclimatic and paleohydrologic record of Mediterranean deep-sea cores based on pteropods, planktonic and benthic foraminifera. Rev Esp Micropaleontol 8: 171–200.

Hiscott RN, Aksu AE, Mudie PJ, Kaminski MA, Abrajano T, Yaşar D, Rochon A (2007a). The Marmara Sea Gateway since ~16 ka: non-catastrophic causes of paleoceanographic events in the Black Sea at 8.4 ka and 7.15 ka. In: YankoHombach V, Gilbert AS, Panin N, Dolukhanov P editors. The Black Sea Flood Question: Changes in Coastline, Climate, and Human Settlement. NATO Science Series IV - Earth and Environmental Sciences. Dordrecht, the Netherlands: Springer, pp. 89–117.

Hiscott RN, Aksu AE, Mudie PJ, Marret F, Abrajano T, Kaminski MA, Evans J, Çakıroğlu A, Yaşar D (2007b). A gradual drowning of the southwestern Black Sea shelf: evidence for a progressive rather than abrupt Holocene reconnection with the eastern Mediterranean Sea through the Marmara Sea Gateway. Quatern Int 167: 19–34.

Imbrie J, Kipp NG (1971). A new micropaleontological method for quantitative paleoclimatology application to a late Pleistocene Caribbean core. In: Turekian KK editor. The Late Cenozoic Glacial Ages. New Haven, CT, USA: Yale University Press, pp. 71–182.

Jorissen FJ, Asioli A, Borsetti AM, Capotondi L, de Visscher JP, Hilgen FJ, Rohling EJ, van der Borg K, Vergnaud Grazzini C, Zachariasse WJ (1993). Late Quaternary central Mediterranean biochronology. Mar Micropaleontol 21: 169–189.

Kallel N, Duplessy JC, Labeyrie L, Fontugne M, Paterne M, Montacer M (2000). Mediterranean pluvial periods and sapropel formation over the last 200 000 years. Paleogeogr Paleoecol 157: 45–58.

Kidd RB, Cita MB, Ryan WBF (1978). Stratigraphy of eastern Mediterranean sapropel sequences recovered during DSDP LEG 42A and their paleoenvironmental significance. In: Hsu KJ, Mondrader L editors. Initial Reports of the Deep Sea Drilling Project. US Government Printing Office, Washington, DC, USA, pp. 421–443.

Lea DW, Pak DK, Spero HJ (2000). Climate impact of Late Quaternary equatorial Pacific sea temperature variations. Science 289: 1719–1724.

Lea DW, Pak DK, Peterson LC, Hughen KA (2003). Synchroneity of tropical and highlatitude Atlantic temperatures over the Last Glacial Termination. Science 301: 1361–1364.

Lisiecki LE, Raymo ME (2005). A Pliocene-Pleistocene stack of 57 globally distributed benthic δ18O records. Paleoceanography 20: 1–17.

Margari V, Pyle D, Bryant C, Gibbard PL (2007). Mediterranean tephra stratigraphy revisited: results from a long terrestrial sequence on Lesvos Island, Greece. J Volcanol Geoth Res 163: 34–54.

Marino G, Rohling EJ, Sangiori F, Hayes A, Casford JL, Lotter AF, Kucera M, Brinkhuis H (2009). Early and middle Holocene in the Aegean Sea: interplay between high and low latitude climate variability. Quaternary Sci Rev 28: 3246–3262.

Melki T, Kallel N, Fontugne M (2010). The nature of transitions from dry to wet condition during sapropel events in the Eastern Mediterranean Sea. Palaeogeogr Palaeoecol 291: 267–285.

Mertens KN, Bradley LR, Takano Y, Mudie PJ, Marret F, Aksu AE, Hiscott RN, Verleye TJ, Mousing EA, Smyrnova LL et al. (2012). Quantitative estimation of Holocene surface salinity variation in the Black Sea using dinoflagellate cyst process length. Quaternary Sci Rev 39: 45–59.

McCorkle DC, Keigwin LD, Corliss BH, Emerson SR (1990). The influence of microhabitats on the carbon isotopic composition of deep-sea benthic foraminifera. Paleoceanography 5: 161–185.

Mommersteeg HJPM, Loutre MF, Young R, Wijmstra TA, Hooghiemstra H (1995). Orbital forced frequencies in the 975,000 year pollen record from Tenagi Philippon (Greece). Clim Dynam 11: 4–24.

Mulitza S, Boltovskoy D, Donner B, Meggers H, Paul A, Wefer G (2003). Temperature: $\delta^{18}O$ relationships of planktonic foraminifera collected from surface waters. Palaeogeogr Palaeoecol 202: 143–152.

Mullineaux LS, Lohmann GP (1981). Late Quaternary stagnations and recirculation of the eastern Mediterranean: changes in the deep water recorded by fossil benthic foraminifera. J Foramin Res 11: 20–39.

Olson DB, Kourafalou VH, Johns WE, Samuels J, Veneziani M (2006). Aegean surface circulation from a satellite-tracked drifter array. J Phys Oceanogr 37: 1898–1917.

Osbourne AH, Marino G, Vance D, Rohling EJ (2010). Eastern Mediterranean surface water Nd during Eemian sapropel S5: monitoring northerly (mid-latitude) versus southerly (sub-tropical) freshwater contributions. Quaternary Sci Rev 29: 2473–2483.

Parker FL (1962). Planktonic foraminifera species in Pacific sediments. Micropaleontology 8: 219–254.

Poulos SE, Drakopoulos PG, Collins MB (1997). Seasonal variability in sea surface oceanographic conditions in the Aegean Sea (Eastern Mediterranean): an overview. J Marine Syst 13: 225–244.

Principato MS, Giunta S, Corselli C, Negri A (2003). Late Pleistocene/Holocene planktic assemblages in three box cores from the Mediterranean Ridge area (WSW of Crete): paleoecological and paleoceanographic reconstruction of sapropel S1 interval. Palaeogeogr Palaeoecol 190: 61–77.

Pujol C, Vernaud-Grazzini C (1995). Distribution patterns of live planktonic foraminifers as related to regional hydrography and productive systems of the Mediterranean Sea. Mar Micropaleontol 23: 187–217.

Reiss Z, Halicz E, Luz B (1999). Late Holocene foraminifera from the SE Levantine Basin. Israel J Earth Sci 48: 1–27.

Retailleau S, Schiebel R, Howa H (2011). Population dynamics of living planktic foraminifers in the hemipelagic southeastern Bay of Biscay. Mar Micropaleontol 80: 89–100.

Rohling EJ (1991). A simple two layered model for shoaling of the eastern Mediterranean pycnocline due to glacio-eustatic sea level lowering. Paleoceanography 6: 537–541.

Rohling EJ, Gieskes WWC (1989). Late Quaternary changes in Mediterranean intermediate water density and formation. Micropaleontology 3: 147–173.

Rohling EJ, Jorissen FJ, Vergnaud Grazzini C, Zachariasse WJ (1993). Northern Levantine and Adriatic Quaternary planktic foraminifera: reconstruction of paleoenvironmental gradients. Mar Micropaleontol 21: 191–218.

Rohling EJ, Jorissen FJ, de Stigter HC (1997). A 200 year interruption of Holocene sapropel formation in the Adriatic Sea. J Micropaleontol 16: 97–108.

Rohling EJ, Sprovieri M, Cane T, Casford JSL, Cooke S, Bouloubassi I, Emeis KC, Schiebel R, Rogerson M, Hayes A et al. (2004). Reconstructing past planktic foraminiferal habitats using stable isotope data: a case history for Mediterranean sapropel S5. Mar Micropaleontol 50: 89–123.

Rosenthal Y, Lohmann GP (2002). Accurate estimation of sea surface temperatures using dissolutioncorrected calibrations for Mg/Ca paleothemometry. Paleoceanography 17: 1044, doi:10.1029/2001PA000749.

Ross CR, Kennett JP (1984). Late Quaternary paleoceanography as recorded by benthonic foraminifera in Strait of Sicily sediment sequences. Mar Micropaleontol 8: 315–336.

Rossignol Strick M (1985). Mediterranean Quaternary sapropels, an immediate response of the African monsoon to variation of insolation. Palaeogeogr Palaeoecol 49: 237–263.

Saito T, Thompson PR, Breger D (1981). Systematic Index of Recent and Pleistocene Planktonic Foraminifera. Tokyo: Univ. Tokyo Press.

Sautter LR, Thunell RC (1991). Seasonal variability in the $\delta^{18}O$ and $\delta^{13}C$ of planktonic foraminifera from an upwelling environment: sediment trap results from the San Pedro basin, southern California big. Paleoceanography 6: doi: 10.1029/91PA00385. issn: 08838305.

Schiebel R, Zeltner A, Treppke UF, Waniek JJ, Bollmann J, Rixen T, Hemleben C (2004). Distribution of diatoms, coccolithophores and planktic foraminifers along a trophic gradient during SW monsoon in the Arabian Sea. Mar Micropaleontol 51: 345–371.

Skliris N, Mantziafou A, Sofianos S, Gkanasos A (2010). Satellite-derived variability of the Aegean Sea ecohydrodynamics. Cont Shelf Res 30: 403–418.

Sperling M, Schmiedl G, Hemleben C, Emeis KC, Erlenkeuser H, Grootes PM (2003). Black Sea impact on formation of eastern Mediterranean sapropel S1? Evidence from the Marmara Sea. Palaeogeogr Palaeoecol 190: 9–21.

Stefanelli S, Capotondi L, Ciaranfi N (2005). Foraminiferal record and environmental changes during the deposition of the Early-Middle Pleistocene sapropels in southern Italy. Palaeogeog Palaeoecol 216: 27–52.

Thom N (2010). A hydrological model of the Black and Caspian Seas in the late Pleistocene and early-middle Holocene. Quaternary Sci Rev 29: 2989–2995.

Thunell RC, Williams DF, Kennett JP (1977). Late Quaternary paleoclimatology, stratigraphy, and sapropel history in eastern Mediterranean deepsea sediments. Mar Micropaleontol 2: 377–388.

Thunell RC (1979). Eastern Mediterranean Sea during the last glacial maximum; an 18000 year BP reconstruction. Quaternary Res 11: 353–372.

Thunell RC, Reynolds LA (1984). Sedimentation of planktonic foraminifera: Seasonal changes in species flux in the Panama Basin. Micropaleontology 30: 243–262.

Tzedakis PC, Andrieu V, de Beaulieu JL, Crowhurst S, Follieri M, Hooghiemstra H, Magri D, Reille M, Sadori L, Shackleton NJ et al. (1997). Comparison of terrestrial and marine records of changing climate of the last 500,000 years. Earth Planet Sc Lett 150: 171–176.

Tzedakis PC, McManus PC, Hooghiemstra H, Oppo DW, Wijmstra TA (2003). Comparison of changes in vegetation in northeast Greece with records of climate variability on orbital and suborbital frequencies over the last 450,000 years. Earth Planet Sc Lett 212: 197–212.

Tzedakis PC, Hooghiemstra H, Palike H (2006). The last 1.35 million years at Tenaghi Philippon: revised chronostratigraphy and long-term vegetation trends. Quaternary Sci Rev 25: 3416–3430.

van der Meer MTJ, Baas M, Rijpstra WIC, Marino G, Rohling EJ, Damsté JSS, Schouten S (2007). Hydrogen isotopic compositions of long-chain alkenones record freshwater flooding of the Eastern Mediterranean at the onset of sapropel deposition. Earth Planet Sc Lett 262: 594–600.

Velaoras D, Lascaratos A (2005). Deep water mass characteristics and interannual variability in the North and Central Aegean Sea. J Marine Syst 53: 59–85.

Vergnaud-Grazzini C, Ryan WBF, Cita MB (1977). Stable isotopic fractionation, climate change and episodic stagnation in the Eastern Mediterranean during the Late Quaternary. Mar Micropaleontol 2: 353–370.

Vidal L, Ménot G, Joly C, Bruneton H, Rostek F, Çağatay MN, Major C, Bard E (2010). Hydrology in the Sea of Marmara during the last 23 ka: implications for timing of Black Sea connections and sapropel deposition, Paleoceanography 25: PA1205, doi:10.1029/2009PA001735.

Wijmstra TA, Young R (1992). Vegetational and climatic transitions between interglacial and glacial periods during the last 1 million years in northern Greece. In: Kukla GJ, Went E editor. Start of a Glacial. Berlin Heidelberg, Germany: Springer, pp. 97–112.

Yaltırak C, İşler B, Aksu AE, Hiscott RN (2012). Evolution of the Bababurnu Basin and shelf of the Biga Peninsula: western extension of the Middle Strand of the North Anatolian Fault Zone, Northeast Aegean Sea, Turkey. J Asian Earth Sci 57: 103–119.

Zaric S, Donner B, Fischer G, Mulitza S, Wefer G (2005). Sensitivity of planktic foraminifera to sea surface temperature and export production as derived from sediment trap data. Mar Micropaleontol 55: 75–105.

Zervakis V, Georgopoulos D (2002). Hydrology and circulation in the north Aegean (eastern Mediterranean) throughout 19971998. Mediterr Mar Sci 3: 7–21.

Zervakis V, Georgopoulos D, Drakopoulos PG (2000). The role of the North Aegean in triggering the recent Eastern Mediterranean climatic changes. J Geophys Res 105 (C11): 26103–26116.

Zervakis V, Georgopoulos D, Karageorgis AP, Theocharis A (2004). On the response of the Aegean sea to climatic variability: a review. Int J Climatol 24: 1845–1858.

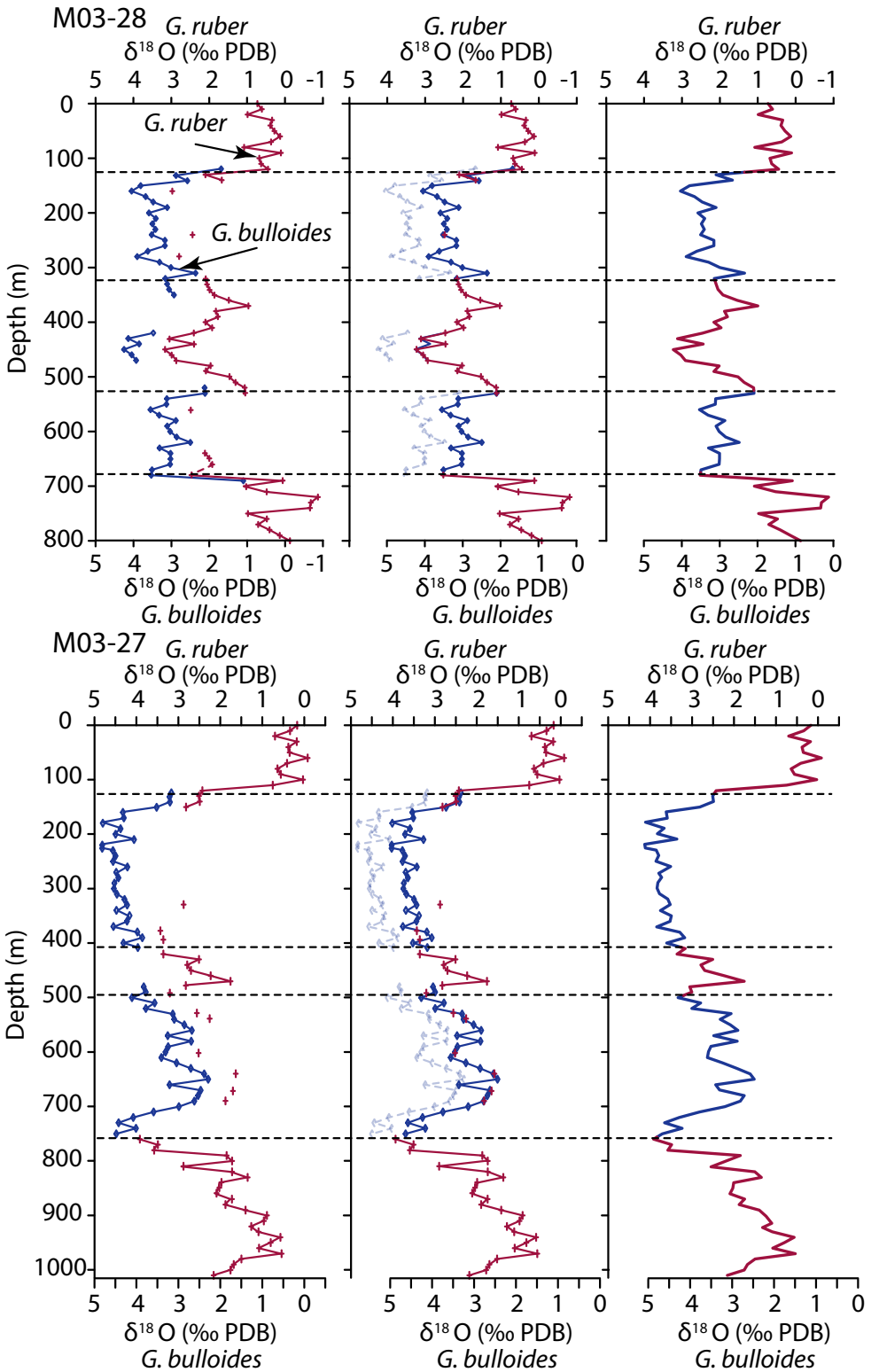


**Appendix 1.** Details of the raw oxygen isotopic data in cores MAR03-27 and MAR03-28, showing the construction of the pseudocomposite plot. Red and blue symbols and lines are the $\delta^{18}O$ values in planktonic foraminifera *G. ruber* and *G. bulloides*, respectively. Note that there are two scales in each graph. The pseudocomposite plot (column on far right) is carried forward into figures requiring the oxygen isotopic records of cores MAR03-27 and MAR03-28.

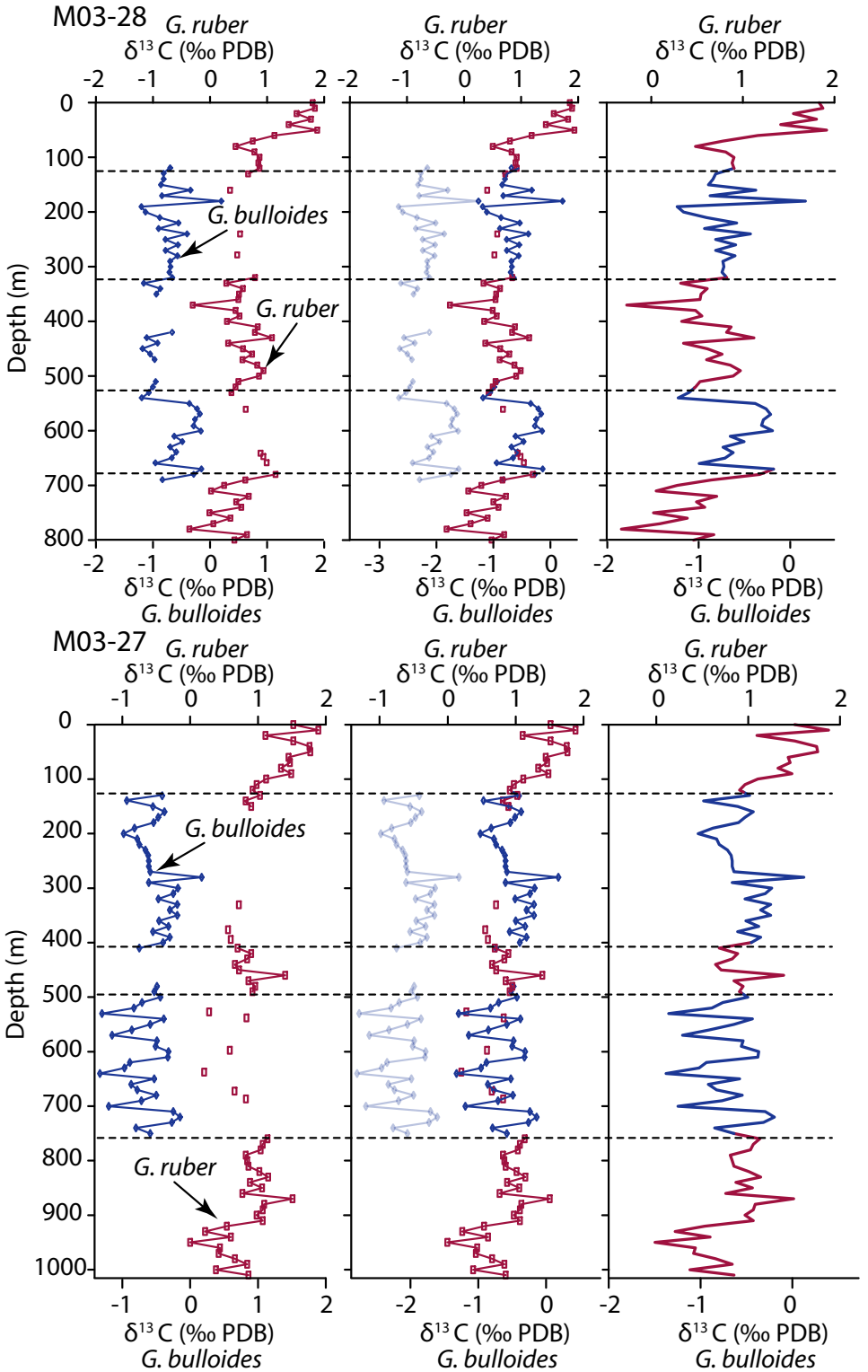


**Appendix 2.** Details of the raw carbon isotopic data in cores MAR03-27 and MAR03-28, showing the construction of the pseudocomposite plot. Red and blue symbols and lines are the $\delta^{13}C$ values in planktonic foraminifera *G. ruber* and *G. bulloides*, respectively. Note that there are two scales in each graph. The pseudocomposite plot (column in far right) is carried forward into figures requiring the carbon isotopic records of cores MAR03-27 and MAR03-28.